



Bruno Miguel de Figueiredo Ramos

Licenciado em Ciências da Engenharia Electrotécnica e de Computadores

Lightly synchronized Multipacket Reception in Machine-Type Communications Networks

Dissertação para obtenção do Grau de Mestre em
Engenharia Electrotécnica e de Computadores

Orientadores: Luis Filipe Lourenço Bernardo, Pr.Dr,
FCT-UNL
Rui Miguel Henriques Dias Morgado Dinis , Pr.Dr,
FCT-UNL

Júri

Presidente: Rodolfo Alexandre Duarte Oliveira, Prof. Dr., FCT-UNL
Arguente: Nuno Manuel Branco Souto, Prof.Dr., ISCTE-IUL
Vogal: Luis Filipe Lourenço Bernardo, Prof.Dr., FCT-UNL



FACULDADE DE
CIÊNCIAS E TECNOLOGIA
UNIVERSIDADE NOVA DE LISBOA

Setembro, 2016

Lightly synchronized Multipacket Reception in Machine-Type Communications Networks

Copyright © Bruno Miguel de Figueiredo Ramos, Faculdade de Ciências e Tecnologia, Universidade NOVA de Lisboa.

A Faculdade de Ciências e Tecnologia e a Universidade NOVA de Lisboa têm o direito, perpétuo e sem limites geográficos, de arquivar e publicar esta dissertação através de exemplares impressos reproduzidos em papel ou de forma digital, ou por qualquer outro meio conhecido ou que venha a ser inventado, e de a divulgar através de repositórios científicos e de admitir a sua cópia e distribuição com objetivos educacionais ou de investigação, não comerciais, desde que seja dado crédito ao autor e editor.

Este documento foi gerado utilizando o processador (pdf) \LaTeX , com base no template “unlthesis” [1] desenvolvido no Dep. Informática da FCT-NOVA [2]. [1] <https://github.com/joaomlorenco/unlthesis> [2] <http://www.di.fct.unl.pt>

To my mother

ACKNOWLEDGEMENTS

I want to start by thanking Prof. Dr. Luís Bernardo, the main reason this dissertation was made possible. I was really lucky to have him as my adviser. He was extremely patient with me and all my technical flaws, in times of extreme pressure, his guidance made things seem easy when they were not.

I'd like to thank the entire telecommunication group. Since my first year at the university that my passion for telecommunications began to grow, and the lectures from this group of professors inspired me alot.

This work was supported by *Fundação para a Ciência e a Tecnologia* (FCT) projects ADIN PTDC/EEI-TEL/2990/2012 and UID/EEA/50008/2013 (*Instituto de Telecomunicações*). I thank them for financing the research scholarship BI_112_15.

I'm thankful to *Universidade Nova de Lisboa, Faculdade de Ciências e Tecnologia* and *Departamento de Engenharia Electrotécnica e de Computadores* for creating the conditions that allowed me to complete my education.

Being a foreign student, I was very lucky to have such wonderful colleagues, David Borges, Ricardo Candeias, Cirilo Zenóglho, Bernardo Albergaria, Daniela Oliveira and many others helped shape this fantastic journey. From intellectual conversations to jokes about everything and everyone, from being in a classroom for 3 hours to partying for 3 hours at Bairro Alto, from group work at a colleagues house to eating ice cream at Costa da Caparica on a hot summer day, nothing would be the same without this really awesome individuals.

I'd like to dedicate a special paragraph to my mother and aunts. They are the reason I am who I am. Extremely hardworking women, they taught me to work hard for my goals, to always want to learn more and, of course, to be respectful to everyone. I can't thank them enough.

A huge thank you to everyone I mentioned.

*"First they ignore you, then they laugh at you, then they
fight you, then you win"*

Anonymous

ABSTRACT

Machine Type Communication (MTC) applications were designed to monitor and control elements of our surroundings and environment. MTC applications have a different set of requirements compared to the traditional communication devices, with Machine to Machine (M2M) data being mostly short, asynchronous, bursty and sometimes requiring end-to-end delays below 1ms. With the growth of MTC, the new generation of mobile communications has to be able to present different types of services with very different requirements, i.e. the same network has to be capable of "supplying" connection to the user that just wants to download a video or use social media, allowing at the same time MTC that has completely different requirements, without deteriorating both experiences. The challenges associated to the implementation of MTC require disruptive changes at the Physical (PHY) and Medium Access Control (MAC) layers, that lead to a better use of the spectrum available. The orthogonality and synchronization requirements of the PHY layer of current Long Term Evolution Advanced (LTE-A) radio access network (based on OFDM and Single Carrier Frequency Domain Equalization (SC-FDE)) are obstacles for this new 5th Generation (5G) architecture. Generalized Frequency Division Multiplexing (GFDM) and other modulation techniques were proposed as candidates for the 5G PHY layer, however they also suffer from visible degradation when the transmitter and receiver are not synchronized, leading to a poor performance when collisions occur in an asynchronous MAC layer. This dissertation addresses the requirements of M2M traffic at the MAC layer applying multipacket reception (MPR) techniques to handle the bursty nature of the traffic and synchronization tones and optimized back-off approaches to reduce the delay. It proposes a new MAC protocol and analyses its performance analytically considering an SC-FDE modulation. The models are validated using a system level cross-layer simulator developed in MATLAB, which implements the MAC protocol and applies PHY layer performance models. The results show that the MAC's latency depends mainly on the number of users and the load of each user, and can be controlled using these two parameters.

Keywords: Machine Type Communication; 5G; Sub-millisecond communication; MAC protocol; Cross-layer optimization; Simulation.

RESUMO

As aplicações para Comunicação do Tipo Máquina (MTC) foram concebidas para monitorar e controlar elementos à volta e do meio ambiente. As aplicações MTC têm um conjunto diferente de requisitos em relação aos dispositivos de comunicação tradicionais, com dados Máquina para máquina (M2M) curtos, assíncronos, em rajadas e, por vezes exigindo atrasos destino a destino abaixo de 1 ms. Com o crescimento da MTC, a nova geração de comunicações móveis tem de ser capaz de apresentar diferentes tipos de serviços com requisitos muito diferentes. A mesma rede tem que ser capaz de ligar o utilizador que só quer baixar um vídeo ou usar redes sociais, permitindo, ao mesmo tempo MTC, que tem exigências completamente diferentes, sem deteriorar ambas as experiências. Os desafios associados à implementação da MTC requerer alterações disruptivas nas camadas Física (PHY) e de controlo de acesso ao meio (MAC), que levam a uma melhor utilização do espectro disponível. Os requisitos de ortogonalidade e sincronização da camada PHY da rede de acesso de rádio atual Long Term Evolution Avançada (LTE-A) (com base nas modulações Orthogonal Frequency Division Multiplexing (OFDM) e Single Carrier-Frequency Domain Equalization (SC-FDE)) são obstáculos para criar a nova 5ª geração (5G) das redes celulares. A Generalized Frequency Division Multiplexing (GFDM) e outras técnicas de modulação foram propostas como candidatas para a camada PHY 5G, no entanto, elas também sofrem de degradação visível quando o transmissor e o recetor não estão sincronizados, o que leva a um fraco desempenho quando ocorrem colisões numa camada MAC assíncrona. Esta dissertação aborda as necessidades do tráfego M2M na camada MAC através da aplicação de técnicas de Receção Multi Pacote (MPR) para lidar com a natureza em rajadas do tráfego, e de tons de sincronização e de abordagens de recuo otimizadas para reduzir o atraso. Ela propõe um novo protocolo MAC e analisa o seu desempenho analiticamente, considerando uma modulação SC-FDE. Os modelos são validados usando um simulador de sistema desenvolvido em MATLAB, que implementa o protocolo MAC e aplica modelos de desempenho camada PHY. Os resultados mostram que a latência do protocolo MAC depende principalmente do número de utilizadores e da carga de cada utilizador, e pode ser controlada usando estes dois parâmetros.

Palavras-chave: Comunicação entre máquinas; 5G; Comunicação em sub-milissegundos; Protocolos MAC; Otimização conjunta de camada; Simulação.

CONTENTS

List of Figures	xvii
List of Tables	xix
Acronyms	xxi
1 Introduction	1
1.1 Research goals and contributions	2
1.2 Dissertation's outline	3
2 Related Work	5
2.1 Introduction	5
2.2 Access Schemes	6
2.2.1 Orthogonal Frequency Division Multiplexing	7
2.2.2 Single-Carrier Frequency Domain Equalization	12
2.2.3 Filter Bank Multicarrier	17
2.2.4 Universal-Filtered Multi-Carrier	20
2.2.5 Generalized Frequency Division Multiplexing	21
2.3 MAC Protocols for MTC communications	23
2.3.1 DPCF-M	27
2.3.2 Scalable Hybrid MAC	28
2.3.3 Adaptative Multichannel Protocol for large-Scale M2M	29
2.3.4 Adaptative Traffic Load Slotted MACA	29
2.3.5 Code Expanded Random Access	30
2.3.6 Enhancement of IEEE 802.11ah for M2M Communications	31
2.3.7 Fast Adaptive Slotted ALOHA	31
2.3.8 LTE-A MAC layer design for MTC	32
2.3.9 M2M MAC protocols overview	32
2.3.10 5GNow Proposed MAC protocol	33
2.4 Multipacket Reception	34
2.4.1 MIMO	35
2.4.2 Network Diversity Multiple Access	36
2.4.3 Successive Interference Cancellation	36

2.4.4	Hybrid automatic repeat request network division multiple access	36
2.4.5	Non-Orthogonal multiple access	37
3	Multipacket reception	39
3.1	Introduction	39
3.2	System Characterization	39
3.2.1	Multipacket detection receiver performance	40
3.3	Accuracy Analysis	42
3.3.1	Packet error rate evaluation	43
3.3.2	Analytical model versus approximate model	44
3.4	Medium access control protocol requirements	46
4	Machine type communications hybrid network diversity multiple access protocol	49
4.1	Introduction	49
4.2	Protocol design	49
4.2.1	Objectives	49
4.2.2	Protocol characterization	50
4.2.3	Packet structure	51
4.2.4	Power Control	52
4.3	Performance Analysis	52
4.3.1	Analytical system model	52
4.4	Simulation Results	57
4.4.1	Simulation scenario	58
4.4.2	Average number of transmissions	58
4.4.3	Network Utilization rate	58
4.4.4	Average Delay	60
4.4.5	Time limit overrun	62
4.4.6	Energy efficiency	64
5	Conclusions	65
5.1	Final considerations	65
5.2	Future work	65
	Bibliography	67
A	Simulator's structure	73
A.1	Global architecture	73
A.2	Distance and channel coefficient	75
A.3	Output	76
B	Article	79

LIST OF FIGURES

2.1	Block Diagram for multicarrier transmission [28]	8
2.2	time representation of OFDM. [13]	9
2.3	OFDM frequency representation [13]	9
2.4	SC-FDMA system block diagram [51]	15
2.5	The HDFFE structure [10]	16
2.6	Block diagram of an FBMC transceiver [17]	18
2.7	Block diagram of an FBMC system using OQAM symbols: SMT [17]	19
2.8	GFDM and OFDM frame Comparision for the MTC scenario [38]	21
2.9	Block diagram of the transceiver [38]	22
2.10	Details of the GFDM modulator [38]	22
2.11	Taxonomy of M2M MAC protocols [46]	25
2.12	DPCF-M protocol frame structure [5]	28
2.13	Frame structure for the contention-TDMA hybrid MAC protocol [34]	28
2.14	Code expanded random access [45]. (a) Current random access in LTE. (b) Code expanded random access. (c) Current LTE random access codewords, with collision for nodes 2 and 3. (d) Code expanded codewords, with phantom codeword in last row. I denotes a node is idle.	30
2.15	The 5G vision of a unified frame for diferent types of traffic [63].	34
2.16	Classification of techniques applied for MPR [35]	35
2.17	H-NDMA MPR scheme [24]	37
3.1	System Model	40
3.2	PER performance for $P=10$, $L=[1,10]$, and 4 iterations	43
3.3	Minimum E_b/N_0 required to transmit successfully with one power level, $P=[1,10]$, $L=[1,10]$, and 4 iterations	44
3.4	PER performance for E_b/N_0 and power offset for $P=10$, $L=5$	45
3.5	Estimated and simulated PER performances comparison for diferent number of MTs using the upper transmission level q_2	45
3.6	Average number of transmissions for $J = [1, 60]$	46
3.7	Relative error between models' average number of transmission evaluation	47
4.1	MTs wake-up radio example	50
4.2	MTC H-NDMA protocol example	51

4.3	MTC H-NDMA protocol example	51
4.4	Maximum J for $\delta_{max} = 100\mu s$	55
4.5	Maximum J for $\delta_{max} \in [50, 300]\mu s$	55
4.6	Average number of transmissions per epoch for $J=[10,50]$	59
4.7	Network utilization ratio (ρ)	59
4.8	Average number of MTs per epoch	60
4.9	Network utilization ratio (ρ) for $J = [200, 1000]$	60
4.10	Network utilization ratio as a function of λ	61
4.11	Average total packet delay $P=[20,60]$	61
4.12	Average total packet delay $J = [100, 1000]$	62
4.13	Average total packet delay as a function of λ for $J = 600, 800, 1000$	62
4.14	Probability of exceeding δ_{max} for $J = \{30, 60\}$ MTs and $\lambda = \{1.0, 1.6\}$ packets/ T_D	63
4.15	Probability of exceeding δ_{max} for $J = \{600, 1000\}$ MTs and $\lambda = \{1.0, 1.6\}$ packets/ T_D	63
4.16	EPUP as a function of J	64
A.1	Simulation flowchart	74
A.2	<i>statsTable</i> for 10 MTs with 200% aggregate uplink load	76
A.3	<i>statsTable</i> for 10 MTs with 200% aggregate uplink load	77

LIST OF TABLES

2.1 Comparison of MAC protocols specific to M2M communication	33
---	----

ACRONYMS

3GPP-LTE The Third Generation Partnership Project-Long Term Evolution.

4G 4th generation.

5G 5th Generation.

AP access point.

app Application.

ATL S-MACA adaptive traffic load slotted MACA.

BER bit error rate.

BS Base Station.

CDMA code division multiple access.

CERA Code Expanded Random Access.

CFOs carrier frequency offsets.

CoMP Coordinated multi-point.

COP contention only period.

CP Cyclic Prefix.

CQI channel quality indicator.

CS cyclic suffix.

CS/CB coordinated scheduling/coordinated beamforming.

CSMA Carrier-Sense Multiple Access.

CSMA/CA Carrier-Sense Multiple Access with collision avoidance.

DC Diversity Combining.

DFT Discrete Fourier Transform.

DPCF-M distributed point coordination function-M.

ELL Extreme low latency.

EPUP Energy Per Useful Packet.

FASA Fast adaptive slotted ALOHA.

FBMC Filter Bank Multicarrier.

FD frequency domain.

FDE Frequency-Domain Equalization.

FDMA Frequency Division Multiple Access.

FFT fast Fourier Transform.

GFDM Generalized Frequency Division Multiplexing.

H-ARQ hybrid ARQ.

H-NDMA Hybrid automatic repeat request Network Diversity Multiple Access.

HDFE hybrid DFE.

IBDFE Iterative Block DFE.

ICI Inter-Carrier Interference.

IDMA interleaving division multiple-access.

IFFT inverse fast Fourier Transform.

IoT Internet of Things.

ISI Inter-Symbol Interference.

JR joint reception.

JT joint transmission.

LTE Long Term Evolution.

LTE-A Long Term Evolution Advanced.

M2M Machine to Machine.

MAC Medium Access Control.

MACA multiple access with collision avoidance.

MCM Multi-Carrier Modulations.

MIMO Multiple Input Multiple Output.

MMC Massive Machine Communication.

MMSE minimum mean-square error.

MPD Multi-Packet Detection.

MPR multipacket reception.

MSE minimum mean square error.

MT Mobile Terminal.

MTC Machine Type Communication.

MUD Multi-User Detection.

NDMA Network-assisted Diversity Multiple Access.

NOMA Non-Orthogonal Multiple Access.

NP notification period.

OFDM Orthogonal Frequency Division Multiplexing.

OFDMA Orthogonal Frequency Division Multiple Access.

OMA Orthogonal Multiple Access.

OOB Out-Of-Bound.

OQAM offset QAM.

OQPSK Offset Quadrature Phase Shift Keying.

P/S parallel to serial.

PAM Pulse Amplitude Modulation.

PCF point coordination function.

PDU protocol data unit.

PHY Physical.

PRACH physical random access channel.

QAM Quadrature Amplitude Modulation.

QPSK Quadrature Phase Shift Keying.

RACH random access channel.

RAW restricted access window.

RFG request for gateway.

RRC radio resource control.

S/P serial to parallel.

SC-FDMA Local Single Carrier FDMA.

SC-FDE Single Carrier Frequency Domain Equalization.

SCM Single-Carrier Modulation.

SIC Successive Interference Cancellation.

SMT staggered multitone.

SNR signal-to-noise ratio.

SOOC self-optimizing overload control.

SPR single packet reception.

TD time domain.

TDMA Time Division Multiple Access.

TOP transmission only period.

TUOS Terminal Unique Orthogonal spreading-Sequence.

UFMC Universal-Filtered Multicarrier.

WINNER Wireless Initiative New Radio.

WRAN Wireless Regional Area Network.

INTRODUCTION

Traditional communications systems have long been used as a means for users to exchange with each other very different types of data: we can now use a smartphone to call a sibling, send a funny video to your friends or share a photo on facebook. In recent years, we have seen a great expansion of the landscape of machine-generated information. There are many new gadgets and devices (e.g. smart-watches) that are potential sources of valuable information. Thanks to advances in communications technology, machines can be connected, reached at an affordable cost and will rapidly become an integral part of the global information network [18]. The growth of machine-type communications, comes as a consequence of our need to steer/control elements of our surroundings and environment, as gadgets, sensors and other machines turns our life easier. Once machines become connected, the next natural leap is to have them controlled remotely, causing a completely new paradigm for control communication [18].

This trend of connecting humans to machines and with other machines is referred to as **MTC** or **M2M** communication. We have seen, over recent years, a multitude of wireless **M2M** applications (e.g. vending machines and public transportation systems), but this type of communication is not yet a commercial success. Fettweis *et al* [18] states that the lack of success of **MTC** is caused by the fact that **M2M** applications have a very different set of requirements when compared to the conventional human-centric network designed to meet the human basic needs of communication with voice, text and video applications.

For **M2M** to reach its full potential it needs a network optimized for it [18]. **MTC** has a particular set of requirements that the current mobile network, **LTE-A**, does not fulfill. The nature of most of this data will mostly be short, bursty, and asynchronous. The cellular network has to be able to handle tens of billions of devices, since the number of these devices is orders of magnitude larger than conventional communication devices of today and this number will only grow with time.

A MAC layer design for M2M communication in LTE-A is presented in [12]. In this article they argue that the overhead associated with the signaling required for the radio resource control (RRC) mechanism used in Long Term Evolution (LTE) is prohibitive in a case such as MTC where devices may have very little data to send. In order to make the channel access mechanism more efficient, they propose a new policy where backlogged nodes first send an access request to the Base Station (BS) using a preamble. When the BS receives the preamble, it allocates uplink resources to the node to send the RRC setup request. In this case, the nodes directly send data in the form of a MAC protocol data unit (PDU), instead of sending a RRC setup request as in LTE-A. The BS is modified to recognize the MAC PDU, which may contain the node identity and security information [46]. Another enhancement is proposed by the authors where the MAC protocol is further simplified by allowing nodes to directly send the data in encoded format along with a special preamble. This proposed simplifications to the MAC layer in LTE-A improve the efficiency and avoid unnecessary control overhead [46]. These proposed designs fail to address successfully all M2M communications requirements, the LTE-A system makes it difficult to efficiently implement MTC communications, as shown in chapter 2.

A new approach is needed when designing the next cellular network system (5th Generation (5G)), if MTC is to be implemented. Wunder *et al* proposed in [63] a unified uplink frame structure. They defend that a 5G approach must be able to efficiently support different traffic types, which all have to be part of future wireless cellular systems. They presented a totally asynchronous scenario for MTC traffic, an interleaving division multiple-access (IDMA)-like approach, is proposed as an appealing candidate to generate these different types of signal layers [63]. In order to correctly solve collisions, this protocol needs to know in advance the number of transmitting nodes, which means, in their totally asynchronous environment, any signal transmitted by a new MTC device would add noise to the system.

The work developed in this dissertation intends to address this new environment introduced in 5G, by defining a new cross-layer PHY/MAC protocol. MPR techniques are applied in the physical layer, and multiple power levels are used for data transmission. The MAC protocol addresses the delay and energy requirements by applying synchronization tones and optimized backoff approaches.

1.1 Research goals and contributions

This brief section states the research problem and respective objectives. The problem is stated as follows:

New modulations and reception paradigms are being developed for sub-millisecond communications, to fulfill the very strict requirement on the delay, together with near asynchronous initial interaction. New protocols are needed for this new environment introduced in 5G.

A cross-layer PHY/MAC protocol is proposed in this thesis, whose goals are:

- Study of the performance of a SC-FDE MPR receiver;
- The definition of a new MAC approach for M2M that uses synchronization tones and optimized backoff approaches adapted to the new scenario.

Both goals were achieved in this dissertation, that contributed with:

- A physical layer analysis of the performance of the MPR SC-FDE system for very large scale systems;
- A MAC protocol named Machine type communications hybrid network diversity multiple access protocol (MTC H-NDMA) was designed and a system level simulator was implemented using MATLAB, which considers the physical layer performance models.

The system composed by the MPR receiver and the MTC H-NDMA protocol presented in chapter 3 and 4 was accepted for publication in the *IEEE GLOBECOM 2016 Workshops* (a reference to the paper is included in Appendix B)

1.2 Dissertation's outline

The dissertation's structure is as follows: Chapter 2 overviews an literature review, describing the related work to the thesis scope. It starts by describing various access schemes that are already deployed and others that are candidates to be used on the next 5G network. A small description of the current state of the art of MPR technology is given, as a possible solution to address the requirements of MTC-oriented networks. Chapter 3 starts by analytically describing the MPR receiver and presents an approximate model for the Packet Error Rate (PER). It then makes an analysis of the receiver performance with a set of simulations, evaluating the optimum gap between transmission power levels needed in order to allow minimum PER and reduce the number of transmissions needed. Finally, it compares the two PER models presented. Chapter 4 describes the MTC H-NDMA protocol that is able to control the system. The performance is evaluated using a set of simulations that measures the system performance in terms of delay, network utilization rate and energy efficiency. Chapter 5 summarizes all conclusions made throughout this dissertation and presents suggestions for future work that can be done in order to improve the system.

RELATED WORK

2.1 Introduction

Researchers were eager to find a killer [Application \(app\)](#) for the next mobile generation ([5G](#)), since they started working on it. Every generation until now had a killer app which made the market of mobile communication grow. There is yet no consensus on this matter, but some of the main drivers have been identified [[63](#)]:

- **Internet of Things (IoT):** This is a very important case of study, given the potential advantages to our society of having almost every object in the world connected to the Internet. On the other hand there are some challenges to overcome, such as the scalability, with a very large number of low-cost and long lifetime [MTC](#) nodes.
- **Gigabit wireless connectivity:** Mobile communication latencies have always followed the demand of the consumers; now with HD and 3D videos the data rates will have to grow to provide a seamlessly experience to the consumer. We now have data rates of hundreds of Mb/s and it is expected that in [5G](#) we reach data rates 10 times inn the order of Gb/s.
- **Tactile Internet:** Based on the tactile sense of the human being, the idea behind this concept is to build a network that allows users to steer and control machines with round-trip communication latencies below 1 ms, that is the time at which the human body can distinguish actions. As shown in [[20](#)], a maximum time budget of 100 μ s is required for the [PHY](#) layer. With current technology it is impossible to achieve this requirement.

This type of communication will be the main focus of this dissertation.

A new PHY layer, with some disruptive changes, is needed in order to provide the users the services depicted previously. With the growth of MTC, the new generation of mobile communications has to be able to present different types of services with very different requirements, i.e. the same network has to be capable of "supplying" connection to the user that just wants to download a video or use social media, allowing at the same time MTC that has completely different requirements, without deteriorating both experiences.

The orthogonality and synchronization requirements of the PHY layer of current LTE-A radio access network (based on Orthogonal Frequency Division Multiplexing (OFDM) and SC-FDE) are obstacles for this new 5G architecture [63]. Orthogonality means that there is no interference in the receiver's signal detection and synchronism means that all transmitting devices have a common clock that guides their processing. When orthogonality is destroyed (as seen in [63] this can happen due to random channel access or multi-cell operation) the noise piles up without bounds in OFDM.

Machines or devices involved in MTC generate sporadic traffic, i.e. they are not always transmitting, and they should not be obligated to follow the synchronization of LTE-A PHY layer. Instead, they should be able to access the network only when there is information to transmit. In [63] the authors conclude that this sporadic traffic should be carried by non-orthogonal waveforms for asynchronous signaling in the uplink.

The LTE-A waveform, with it's guard bands to other legacy networks, damages spectral efficiency and can even prevent band usage [63]. In this new scenario of uncoordinated interference, a new waveform is needed. This new waveform must have sharp frequency notches and tight spectral masks in order to prevent interference with legacy systems, and must be able to handle uncoordinated interference and asynchronous signaling [63].

As stated before, future applications such as tactile internet requires ultra-low latencies compatible to the human tact sense. With LTE-A offering latencies in the order of multiples of 10ms, new 5G layers and access control protocols are required. All elements of communication have to be optimized in order to achieve ultra-low latency [63].

This chapter describes all related work on this area. It starts by describing existing PHY layer access schemes that are candidates for the 5G PHY layer, then it gives an overview of M2M MAC protocols and, finally, a description of MPR techniques is given.

2.2 Access Schemes

This section starts by describing OFDM and SC-FDE, then it describes PHY layer protocols that are proposed as candidate for future mobile networks: Filter Bank Multicarrier (FBMC), Universal-Filtered Multicarrier (UFMC) and GFDM.

2.2.1 Orthogonal Frequency Division Multiplexing

OFDM is the PHY layer protocol used in LTE and LTE-A 4th generation (4G) mobile phone standards and by others wireless standards (Wi-Max, IEEE802.11a, DVB). This technology is a form of Multi-Carrier transmission and has satisfactory results for frequency selective channels and high data rates [13].

2.2.1.1 The multicarrier transmission concept

The multicarrier concept that brings great advantages to this system is a way to overcome the limitations of linear single carrier modulations (e.g M-PSK or M-QAM), where the bit rate is limited by the delay spread of the channel ¹. As explained in [28], to overcome this limitation the data stream is splitted into K substream of lower data rates and these data substreams are transmitted on adjacent subcarriers. The total bandwidth needed is not affected: each subcarrier has a bandwidth B/K , while T_s is K times higher, allowing for K times higher data rate for a given delay spread ². In OFDM the subcarriers are orthogonal. When this feature is preserved we have a system that is robust against large delays spreads [13].

There are two ways to implement multicarrier transmission. The first one has K individual carriers that are modulated independently. The second one is based on a filter bank of K adjacent bandpass filters that are excited by a parallel data stream. The two implementations differ slightly from the conceptual point of view. Since the second concept point of view is, especially for the case of OFDM, closer to implementation, it will be described with detail the second one and later discuss the first setup.

In Figure 2.1 the Block diagram for the second setup is depicted. We start with a base transmit pulse $g(t)$. We obtain frequency-shifted replicas of this pulse as:

$$g_k(t) = e^{j2\pi f_k t} g(t), \quad (2.1)$$

where f_k is the frequency of the subcarrier. For each time instant l , the set of K(or K+1) modulation symbols is transmitted by using different pulse shapes $g_k(t)$: the parallel data stream excites a filter bank of K (or K + 1) different bandpass filters [28]. The filter outputs are then summed up before the transmission. The transmit signal in the complex baseband is given by

$$s(t) = \sum_l \sum_k s_{kl} g_k(t - lT_s), \quad (2.2)$$

¹For a transmission with delay spread τ_m and symbol duration T_s , the reception without Inter-Symbol Interference (ISI) is only possible if $\tau_m \ll T_s$. Since the bit rate is given by $R_b = \log_2(M)T_s^{-1}$ we can conclude that the delay spread limits the data rate.

²The K factor cannot be increased arbitrarily, because the symbol duration would be too large, making the transmission too sensitive against time incoherence of the channel that is related to the maximum Doppler frequency ν_{max} [28]. The condition $\nu_{max}T_s \ll 1$ has to be fulfilled.

where $s_{kl}(t)$ are the complex modulation symbols, k is the frequency index, l is the time index and T_s is the parallel symbol duration. It is defined

$$g_{kl}(t) = g_k(t - lT_s) = e^{j2\pi f_k(t - lT_s)} g(t - lT_s) \quad (2.3)$$

to get the expression

$$s(t) = \sum_{kl} s_{kl} g_{kl}(t) \quad (2.4)$$

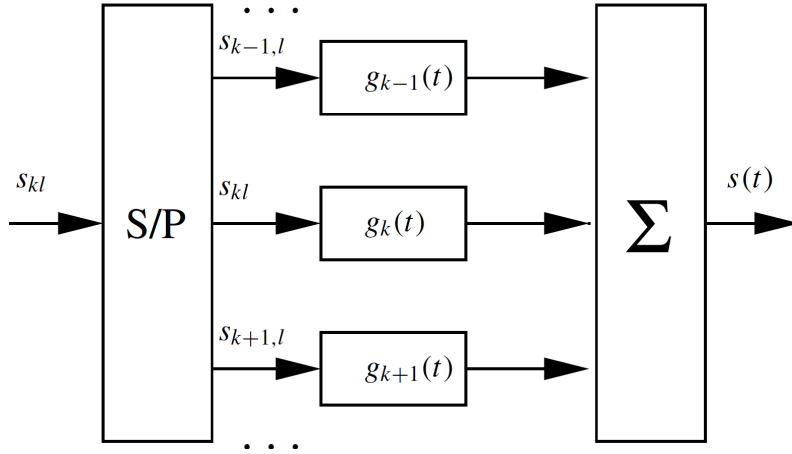


Figure 2.1: Block Diagram for multicarrier transmission [28]

As told before, even though the two setups are mathematically closely related, they have different conceptual points of view. The second setup - the filter bank - is closer to implementation where the filter bank can be implemented with [fast Fourier Transform \(FFT\)](#) [28].

2.2.1.2 OFDM transmission

In [28] the authors show that it is very convenient to have an orthogonal transmit base. The shape of the base transmission pulse $g(t)$ is chosen in a way that they are orthogonal in time and frequency, i.e, it is required that

$$\langle g_{kl}, g_{k'l'} \rangle = \delta_{kk'} \delta_{ll'}, \quad (2.5)$$

where δ is the Kronecker delta given by

$$\delta_{kl} = \begin{cases} 0, & \text{if } k \neq l \\ 1, & \text{if } k = l. \end{cases} \quad (2.6)$$

The orthogonality ensures that the modulation symbol can be recovered from the transmit signal without [ISI](#), i.e. the detector of the receiver will only have s_{kl} as its output.

On a transmission scheme, retrieving s_{kl} from (2.4) is one of the main concerns. In this process, called equalization, s_{kl} is difficult to extract mostly due to the frequency selectivity behavior of the channel [13]. OFDM transmissions' main objective is to turn the channel convolutional effect of (2.4) into a multiplicative one in order to simplify the equalization process. To circularize the channel effect, OFDM schemes add redundancy known as **Cyclic Prefix (CP)**. Knowing that circular convolution can be diagonalized in an FFT basis [13], the multi-path **time domain (TD)** channel is transformed into a set of parallel frequency channels. Due to these advantages, it is appropriate to use OFDM when we have frequency selective channels [13]. Figure 2.2 shows the effect of the CP on OFDM time representation.

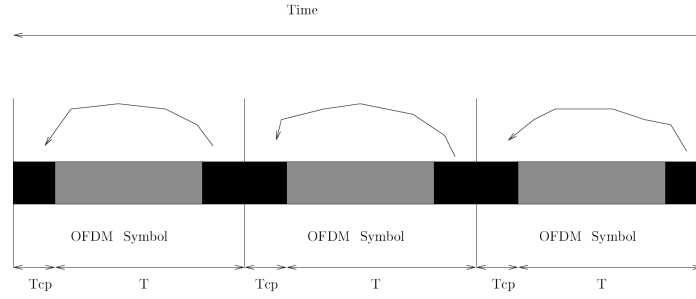


Figure 2.2: time representation of OFDM. [13]

In figure 2.3 we can see the frequency representation of OFDM with N subcarriers. The reader can notice the orthogonality of the subcarriers, since at the frequency where a subcarrier reaches its maximum value, the others subcarriers cancel out when there is no **Inter-Carrier Interference (ICI)**.

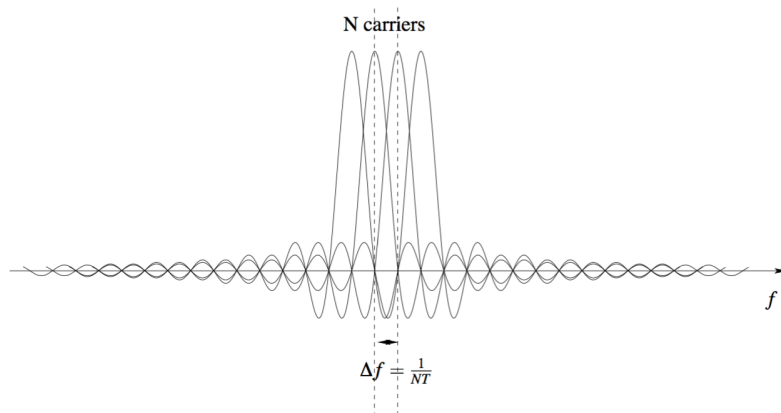


Figure 2.3: OFDM frequency representation [13]

2.2.1.3 Coordinated multi-point (CoMP)-OFDM

As we have seen earlier, **ICI** is an issue that every access schemes tries to mitigate. In recent years, **CoMP** communication techniques have been proposed for **OFDM** systems in order to reduce the **ICI** and boost the system performance [59]. **CoMP** is a good solution for **ICI** in multi-cell wireless networks where many **BS** are spread around an area and they have to cope with multiple users transmission and reception. **CoMP** proposes the cooperation between **BS**, where the cooperation can be considered in transmission of data in downlink or in reception of multiple users signals in uplink. The **CoMP** in these cases is achieved as follows:

- Downlink **CoMP** mainly uses **joint transmission (JT)** or **coordinated scheduling/coordinated beamforming (CS/CB)** approaches to cancel, with efficiency, the interference [59].
- In the uplink case, **CoMP** performs **joint reception (JR)** where multiple **BSs** simultaneously process the received signals from terminals to improve the quality of received information [59] [1].

CoMP-OFDM systems are sensitive to multiple **carrier frequency offsets (CFOs)** between terminals and **BSs** [59]. When **CFOs** occurs in **CoMP-OFDM**, it destroys the orthogonality between **OFDM** subcarriers and causes **ICI** at the receiver, which leads to significant system performance degradation [37] [36] [32]. The **ICI** appears in **OFDM** due to high sidelobe levels of subcarrier spectrum.

2.2.1.4 Pros and Cons of OFDM

OFDM transforms a frequency selective channel into several flat fading channels using **CP**, which brings advantages to this technology. **OFDM** is widely adopted because of the advantages that it offers :

- The orthogonality of subcarrier signals allows:
 - trivial generation of transmit signal through an **inverse fast Fourier Transform (IFFT)** block [17];
 - trivial separation of the transmitted data symbols at the receiver through a **FFT** block [17];
 - trivial equalization through a scalar gain per subcarrier [17];
 - trivial adoption to **Multiple Input Multiple Output (MIMO)**; channels [17].
- For a certain delay spread, the complexity of an **OFDM** modem vs. sampling rate grows slower than the complexity of a single carrier system with an equalizer³ (due to the use of redundancy) [13].

³This technique is described in section 2.2.2

- It is easy to determine the channel attenuations in the frequency domain using a learning sequence [11, 41], or using blind estimation methods [6, 58].
- The spectral efficiency is increased, since subcarriers are overlapped (compared to FDMA systems) [13].
- Adaptive modulation schemes can be applied to subcarrier bands to maximize bandwidth efficiency/transmission rate [17].
- The very special structure of OFDM symbols simplifies the task of carrier and symbol synchronization [17].

As any other technologies, OFDM also has its weakness in comparison to its single-carriers counterparts:

- OFDM does not take advantage of channel diversity, that prohibits the use of plain OFDM schemes in fading environments. If we compare an OFDM system with a single-carrier system using the same error control code in a signal environment rich in diversity, the diversity achieved in OFDM is less than the one achieved by single-carrier systems [13]. Indeed the transmitted information on one OFDM subchannel, due to frequency flat fading, can be irremediably lost if a deep fade occurs [40].
- The baseband transmitted signal can show significant amplitude fluctuations over time, causing the generation of high input backoff ratio at the amplifier of the transmitter [13].
- Finally, the orthogonality in OFDM only occurs when the channel length is smaller than the CP. If this is not the case, some Inter-Carrier Interference occurs, making the orthogonality between subcarriers only approximative [13].
- Only works well in the network downlink of a BS, where all of the subcarriers are transmitted from the same point [17].
- In a cognitive radio setting- where both primary (noncognitive nodes) and secondary users(cognitive nodes) transmit independently and may be based on different standards-the only way to separate the primary and secondary user signal is through a filtering mechanism [17]. OFDM is thus a poor fit because the filters associated with the transmitted and received subcarriers have relatively large side lobes and such lobes will result in leakage of signal powers among the bands of different users [16].

The multi-user version of OFDM is called **Orthogonal Frequency Division Multiple Access (OFDMA)**. Multiple access is achieved in OFDMA by assigning subsets of subcarriers to individual users. This allows simultaneous low data rate transmission from several users. This technique further improves OFDM robustness to fading and interference.

2.2.2 Single-Carrier Frequency Domain Equalization

In the last years, **Single-Carrier Modulation (SCM)** has been getting a lot of attention as an possible alternative to **Multi-Carrier Modulations (MCM)** that are used nowadays in many wireless communication systems (e.g. **OFDM**). One of the main reasons is the use of nonlinear equalizer structures implemented to some extent in the frequency domain by using **FFT**, bringing the complexity close to that of **OFDM** [10].

SC-FDE is a **SCM** combined with **Frequency-Domain Equalization (FDE)**. It is an alternative solution to the **ISI** problem. Equalization - the compensation of the linear distortion caused by channel frequency selectivity- is crucial in digital communications systems. Traditionally **ISI** has been mitigated by *linear equalizers* that implement equalization in the **TD**. Due to the tradeoff between equalization of the channel impulse response to remove **ISI** and noise enhancement at the decision point, a linear equalizer does not have the best performance in terms of bit error rate. [10] proposes nonlinear equalizers with a linear filter to remove part of the **ISI**, followed by a canceler of the remaining interference by using previous detected data. With the use of nonlinear equalizers the capacity of **SCM**, in highly dispersive channels, is similar to that of **OFDM**.

Before presenting nonlinear equalization methods, we will start by describing the system definitions and properties.

2.2.2.1 System Definition and transmission format

A **SCM** signal is generated as a sequential stream of data symbols, at normal time instants nT for $n = \dots, 0, 1, 2, \dots$, where T is the data symbol interval, and $1/T$ is the symbol rate. The **SCM** transmission system is described in [10] using a discrete-time model, where the channel is characterized by the impulse response, in a **MIMO** environment, $h_l^{(j,i)}$, $l = 0, 1, \dots, N_h - 1$, obtained by sampling the cascade of the transmit filter, the channel and the receive filter. Having $s_n^{(i)}$ as the symbol transmitted from the i th antenna, the received signal after sampling at antenna j is given by [10]

$$r_n^{(j)} = \sum_{i=1}^{N_T} \sum_{l=0}^{N_h-1} h_l^{(j,i)} s_{n-l}^{(i)} + w_n^{(j)}, \quad (2.7)$$

where $w_n^{(j)}$ is the noise term with variance σ_w^2 , and $h_l^{(j,i)}$ is the impulse response of the channel from antenna i to antenna j . Given that this dissertation addresses only terminals with single antennas, for simpler notation, from now on, single-input-single-output case will be used, dropping the antenna index in (2.7).

The convolution in (2.7) must be circular in order to allow frequency domain block equalization of the received signal. This can be achieved in different ways, as will be shown next.

Circular and Linear Convolution

Let s_n be the transmitted signal that depends on the information signal d_n (but the two may be different in general). [10] examines cases where each linear convolution in (2.7) appears as a circular convolution between the channel impulse response and the information data signals d_n .

If we consider d_n in blocks of M symbols, the N_h -size sequence h_n , with $M > N_h$, and if we define the periodic signals of period P ⁴, $d_{rep,n} = d_{(n \bmod P)}$, and $h_{rep,n} = h_{(n \bmod P)}$, the circular convolution between d_n and h_n is a periodic sequence of period P defined as [10],

$$x_n^{(circ)} = (h \otimes d)_n = \sum_{l=0}^{P-1} h_{rep,n-l} d_{rep,l}, \quad (2.8)$$

The linear convolution with $n = 0, 1, \dots, M + N_h - 2$ is

$$x_n^{(lin)} = \sum_{l=0}^{N_h-1} h_l d_{n-l}, \quad (2.9)$$

Comparing (2.9) with (2.8), we can easily see that only if $P \geq M + N_h - 1$, then [10]

$$x_n^{(lin)} = x_n^{(circ)} \quad (2.10)$$

Nevertheless, there other conditions (listed below) that yield a *partial equivalence* between the circular convolution and the linear convolution [10], defined by

$$x_n = \sum_{l=0}^{N_h-1} h_l s_{n-l}, \quad (2.11)$$

where s_n depends on d_n .

Overlap and Save: If we consider $s_n = d_n, n = 0, 1, \dots, M - 1$ as the transmitted signal and assumes $P = M$, the equivalence between the linear and the circular convolution holds always on a subset of the computed points [10].

Cyclic Prefix: Instead of considering the transmission of the data sequence d_n , we use an extended sequence s_n obtained by partially repeating d_n with a CP of $L \geq N_h - 1$ samples, [7]:

$$s_n = \begin{cases} d_n, & n = 0, 1, \dots, M - 1 \\ d_{M+n}, & n = -L, \dots, -2, -1. \end{cases} \quad (2.12)$$

Assuming $P=M$, it is easy to prove that (2.11) coincides with (2.8) for $n = 0, 1, \dots, M - 1$, [10]. This arrangement is used in multicarrier communications.

⁴in order to avoid time aliasing, $P \geq M$ and $P \geq N_h$

Pseudo Noise (PN) Extension: Considering a sequence s_n obtained by d_n with the addition of a fixed sequence p_n , $n = 0, 1, \dots, L - 1$, of $L \geq N_h - 1$, [10]:

$$s_n = \begin{cases} d_n, & n = 0, 1, \dots, M - 1 \\ p_{n-M}, & n = M, \dots, M + L - 1. \end{cases} \quad (2.13)$$

The sequence p_n can contain any symbol sequence, including all zeros [53], [49], [50], or a PN symbol sequence, denoted PN extension [10]. Channel estimation also influences the choice of the extension [14].

Some of the advantages of this format are a simple channel estimation, by using the PN sequence [14], and the possibility of implementing an efficient frequency domain (FD) nonlinear equalizer as shown in [10]. PN extensions yield a reduced bit error rate (BER) in comparison to CP as explained in [10].

Signal Generation

A description is given in [10] for the generation of a SCM signal block that proceeds as follows. After coding and serial to parallel (S/P) conversion, blocks of N coded symbols are mapped to the FD by a N -point Discrete Fourier Transform (DFT). The resulting FD data components are mapped by the *pre-matrix time-frequency-space selector* to a set of $M \geq N$ data-carrying subcarriers, and then handled by a M -point inverse DFT to convert back to the TD. The obtained samples are parallel to serial (P/S) converted and a prefix or extension is added for transmission. In Fig. 2.4 the transmission and reception blocks are shown. The simplest frequency mapping is to N contiguous subcarrier frequencies, with the remaining $M - N$ being padded with zeros [10]. In this circumstance, the output samples are expressed as [10]

$$s_n = \frac{1}{M} \sum_{l=0}^{N-1} d_l \sum_{p=0}^{N-1} e^{j2\pi p(n-l)\frac{M}{N}} = \sum_{l=0}^{N-1} g(n-l\frac{M}{N}) d_l, \quad n = 0, 1, \dots, M - 1, \quad (2.14)$$

where

$$g_n = e^{j2\pi \frac{(N-1)n}{M}} \frac{1}{M} \frac{\sin(\frac{\pi N n}{M})}{\sin(\frac{\pi n}{M})} \quad (2.15)$$

and s_n , $n = -L, -L + 1, \dots, -1$, contains the CP. When SCM signals are generated in this way, they are called Local Single Carrier FDMA (SC-FDMA) by the The Third Generation Partnership Project-Long Term Evolution (3GPP-LTE) standards body [39] and DFT pre-coded OFDM by the Wireless Initiative New Radio (WINNER) project [31]. DFT-OFDM has been proposed by WINNER as the uplink transmission format for wide area cellular scenarios, mainly due to its radio frequency impairment robustness properties [10]

In [10] we can find an overview of variations of this procedure.

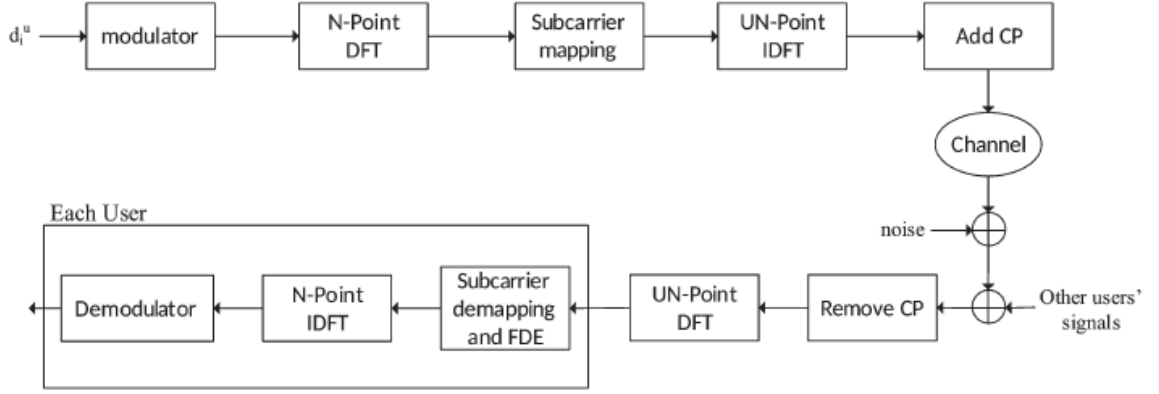


Figure 2.4: SC-FDMA system block diagram [51]

2.2.2.2 Direct Equalization Methods

This section presents equalization structures whose parameters are designed directly from an estimate of the channel frequency response. We will focus on the structure of Decision Feedback Equalizer with a Hybrid Time-Frequency, since this equalizer will be of great importance for the thesis results.

Decision Feedback Equalizer With a Hybrid Time-Frequency Structure

This structure is called **hybrid DFE (HDFE)**, the feedforward filter operates in the **FD** on blocks of received signal, while the feedback operates in the **TD** [8], [15]. Instead of using **CP**, data transmission with a PN extension (presented in the previous section, see (2.13)) must be considered to allow **TD** implementation of the feedback filter [10]. Fig. 2.5 shows **HDFE** structure, where we can see the different stages of equalization. After the **DFT** of the received signal, R_o is obtained and then applied to the feedforward filter, with coefficients C_p , $p = 0, 1, \dots, P - 1$ yielding the block signal Z_p , $p = 0, 1, \dots, P - 1$ [10],

$$Z_p = C_p R_p, \quad p = 0, 1, \dots, P - 1. \quad (2.16)$$

After passing through the inverse **DFT**, Z_p is transformed in to the **TD** to provide z_n . From the detected data sequence \hat{d}_n and (2.13), the extended detected sequence \hat{s}_n is given by [10]

$$\hat{s}_n = \begin{cases} \hat{d}_n, & n = 0, 1, \dots, M - 1 \\ p_{n-M}, & n = M, M + 1, \dots, P - 1. \end{cases} \quad (2.17)$$

If $b_l, l = 1, 2, \dots, N_{FB}$, are the coefficients of the feedback filter, the signal at the input of the decision element is [10]

$$\check{d}_n = z_n + y_n, \quad n = 0, 1, \dots, M - 1 \quad (2.18)$$

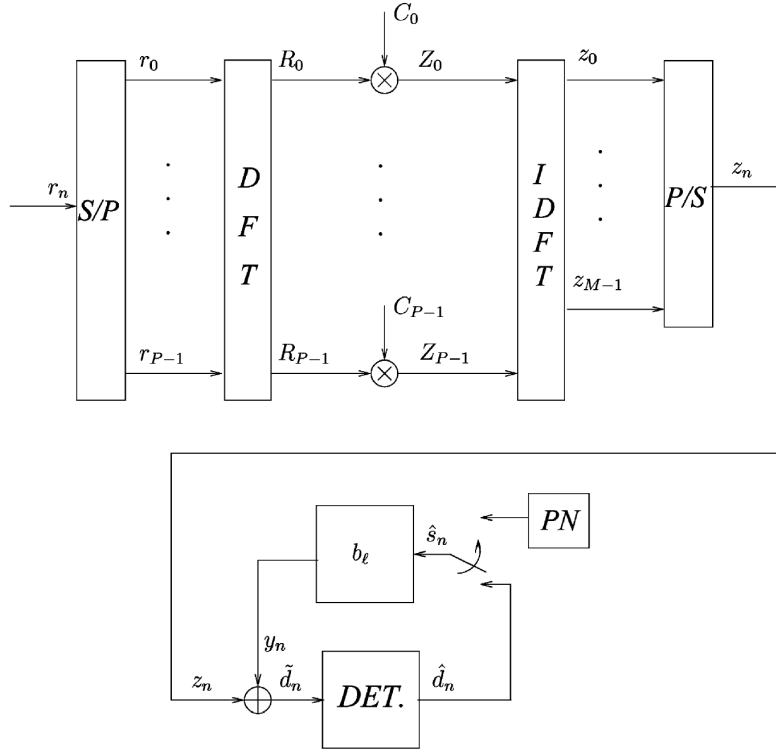


Figure 2.5: The HDFE structure [10]

and

$$y_n = \sum_{l=1}^{N_{FB}} b_l \hat{s}_{n-l} \quad (2.19)$$

is the feedback signal.

The computational complexity of the HDFE structure is $(P/M)\log_2(P) + N_{FB} - (P/M)$ [10].

Let us now describe, starting from the channel frequency response, two design methods for the receiver: zero forcing and minimum mean square error (MSE).

Zero Forcing: All interference must be canceled by the feedback filter [10]. If we define $B_p, p = 0, 1, \dots, P-1$, the feedforward filter is given by [8]

$$C_p = \frac{1}{H_p}(1 - B_p), \quad (2.20)$$

Let \mathbf{A}_{ZF} denote the $N_{FB} \times N_{FB}$ Toeplitz matrix, having as first row the first N_{FB} coefficients of the DFT of $1/|H_p|^2, p = 0, 1, \dots, P-1$ [10]. Let us also define the N_{FB} -size column vector \mathbf{v}_{ZF} , having as elements the first N_{FB} coefficients of the inverse DFT of $1/|H_p|^2, p = 0, 1, \dots, P-1$ [10]. Then, the feedback filter that removes interference is the solution of the linear system $\mathbf{A}_{ZF} \mathbf{b} = \mathbf{v}_{ZF}$ [8].

Minimum Mean Square Error: In this criterion, the coefficients of the feedforward and feedback filters are chosen to minimize the sum of the power of the filtered noise, and the

power of the residual interference [10]. The MSE at the detection point is given by [10]

$$J = E[|\check{d}_n - d_n|^2]. \quad (2.21)$$

[10] shows that, by the Parseval's equation, and by assuming that a) the past detected data symbols are correct $\hat{S}_p = S_p$; b) both noise and data symbols are i.i.d. (independent and identically distributed) and statistically independent of each other; then J is given by

$$J = \frac{1}{p^2} \sum_{p=0}^{P-1} |C_p H_p - B_p - 1|^2 \sigma_D^2 + |C_p|^2 \sigma_W^2, \quad (2.22)$$

where σ_W^2 is the variance of the data in FD.

In [8] the authors show that, setting the gradient J with respect to C_p , $p = 0, 1, \dots, P-1$, to zero, yields a relation between feedforward and feedback coefficients given by

$$C_p = \frac{H_p^*(1 - B_p)}{|H_p|^2 + \frac{\sigma_W^2}{\sigma_D^2}}, \quad p = 0, 1, \dots, P-1. \quad (2.23)$$

Let us define the N_{FB} -size Toeplitz matrix \mathbf{A}_{MMSE} whose first row comprises the first N_{FB} coefficients of the DFT of $\frac{1}{\sigma_D^2 |H_p|^2 + \sigma_W^2}$, $p = 0, 1, \dots, P-1$ and the column vector \mathbf{v}_{MMSE} whose N_{FB} elements are the first N_{FB} coefficients of the IDFT of $\frac{1}{\sigma_D^2 |H_p|^2 + \sigma_W^2}$, $p = 0, 1, \dots, P-1$ [10]. Substituting (2.23) into (2.22) and making the gradient of J equal to zero with respect to the feedback coefficients \mathbf{b} , it is seen that \mathbf{b} is the solution of the linear system of N_{FB} equations and N_{FB} unknowns $\mathbf{A}_{MMSE} \mathbf{b} = \mathbf{v}_{MMSE}$. The complexity of the MSE method is similar to the zero forcing [10].

In [10] we can find an overview of others direct equalization methods, and a comparison between them.

2.2.3 Filter Bank Multicarrier

In section 2.2.1 we described the OFDM systems which has been the dominant technology for broadband multicarrier communications [17]. However, there are certain applications where OFDM is not the best solution (e.g cognitive radios and uplink of multiuser multicarrier system). In this section we will address an alternative to OFDM: FBMC, which some believe is a more effective solution [17]. FBMC, which has been studied even before the invention of OFDM, has been getting a lot of attention lately by a number of researchers. In this section this system will be described.

2.2.3.1 A unified formulation for OFDM and FBMC

There are some similarities between FBMC and OFDM. The FBMC transceiver (block diagram depicted in Fig. 2.6) can be also used in an OFDM setting. The difference between OFDM and FBMC lies on the choice of T (symbol duration) and the transmitter and receiver prototype filters $p_T(t)$ and $p_R(t)$ respectively [17]. In OFDM these prototype

filters are a rectangular pulse height one, with $p_T(t)$ having a duration of T . The receiver prototype filter $p_R(t)$ has a lower width compared to the transmitter filter [17]. FBMC systems are designed for maximum bandwidth efficiency, but the durations of $p_T(t)$ and $p_R(t)$ are greater than T , which causes, in FBMC, the overlapping of successive data symbols [17].

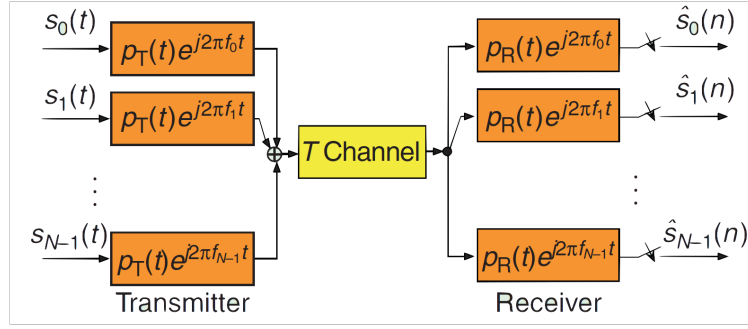


Figure 2.6: Block diagram of an FBMC transceiver [17]

The selection of $p_T(t)$ and $p_R(t)$ depends on the adopted FBMC modulation technique. [17] describes two classes of FBMC system. The first class is designed to transmit **Quadrature Amplitude Modulation (QAM)** data symbols (complex-valued) and the second class is designed to transmit **Pulse Amplitude Modulation (PAM)** data symbols (real-valued). A short overview of these classes is presented next.

FBMC systems for QAM symbol transmission

As we showed on the OFDM section, successive data symbols are isolated through the use of CP. This characteristic of OFDM system constitutes a loss of bandwidth efficiency. This class of FBMC design allows orthogonality of different modulated data symbols without the use of CP. This has the potential of achieving a higher bandwidth efficiency than OFDM [17].

When designing FBMC systems, one of the goals is to design prototype filters that are robust under doubly dispersive channels. In [17] we can find the various designs procedures for this system.

FBMC systems for PAM symbol transmission

The symbol rate can be doubled and also the symbol spacing along the frequency axis can be halved in the FBMC system with PAM symbol transmission (used when data symbols are real-valued), which means that the density of data symbols in the time-frequency phase-space lattice can be quadrupled [17]. But it is worth noticing that PAM transmission can achieve a data symbol density which is twice that of QAM transmission.

Figure 2.7 presents a **staggered multitone (SMT)**⁵ system structure that can be used for **PAM** symbol transmission. The **QAM** symbols (that are divided into its real-part and imaginary-part) may be thought of as the elements of a pair of **PAM** sequences that are then transmitted with a time offset of half the duration of the symbol [17]. This is the most efficient **FBMC** design [59].

In [17] we can find the design procedures for this system as for others alternatives.

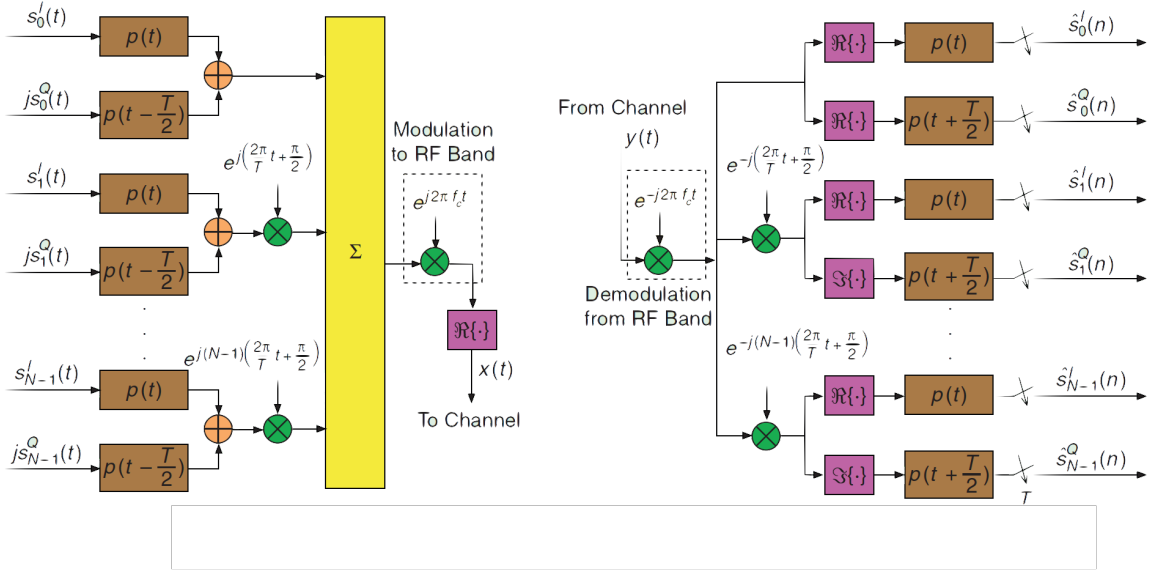


Figure 2.7: Block diagram of an FBMC system using OQAM symbols: SMT [17]

2.2.3.2 FBMC's advantages over OFDM

While **OFDM** is easier to implement and is more robust to timing offset [17], **FBMC** has a number of advantages that makes it more suitable for future communication systems. We will now identify areas where **FBMC** outperforms **OFDM**:

- The uplink of an **OFDMA** network, needs an almost perfect carrier synchronization of signals from different nodes. This is very hard to achieve in practice, particularly in mobile networks. In **FBMC** systems, the signal separation is achieved through filtering, avoiding the need for close to perfect carrier synchronization. Timing synchronization between different users is also avoided since the separation between them is done through a filtering process [17].
- The filtering capability of **FBMC** systems makes them the perfect choice, in cognitive radios, for filling in the spectrum holes [17].

⁵this system has often been referred to as **OFDM-offset QAM (OQAM)**, where **OQAM** stands for offset **QAM**

- **OFDM** is sensitive to fast variations of the communication channels. On the contrary, **FBMC** systems can be designed to be equally robust to channel time and frequency spreading [17].
- **FBMC**'s prototype-filters make this modulation a perfect match to applications where the channel is subject to a number of high-power interfering narrow-band signals [17].

2.2.4 Universal-Filtered Multi-Carrier

OQAM systems (**FBMC**) introduced in previous section, ensure a much lower side-lobe level compared to **OFDM**. While this works well with single-cell, single user transmission, in the uplink case, additional interference paths appear between the interlaced **OQAM** symbol [59]. As we have seen earlier, future wireless communication systems will have to support **MTC** and **IoT**, where these systems will have to support transmission of small data packet. A physical layer that is able to fulfill this target demands efficient support of short transmission bursts. **FBMC/OQAM**, due to its long filter lengths, is not an efficient solution.

UFMC is a multicarrier transmission scheme proposed to overcome the problem of **ICI** in **OFDM** systems. This technique is a generalization of filtered **OFDM** [17] (where the filtering is done on a subcarrier level), i.e, an entire sub-band, that comprises multiples subcarriers, is filtered. One of the design criteria of **UFMC** is to collect the advantages of filtered **OFDM** and **FBMC** while avoiding the respective disadvantages [63]. By using this technique, the effect of sidelobe interference on the immediate adjacent subchannels can be significantly reduced [59]. Other advantage of **UFMC** technique is the use of shorter filter lengths ⁶ compared to **OFDM CP** lengths, which makes it suitable for short burst communication [59].

In [63] they provide simulations that show the superiority of **UFMC** over **OFDM** in a scenario where different traffic types are served by the network, both synchronous and asynchronous. **UFMC** uses filters that are Dolph-Chebyshev-shaped (with 40 dB side-lobe which comes on top of the sinc-shaped spectralside-lobe level attenuation) [63]. For delays greater than **CP**, **UFMC** has a much better performance than **OFDM** [63]. Moreover, it has a symmetric characteristic of **MSE** vs delay, which allows better support of open-loop timing control mechanisms (desirable in **MTC** where we do not want to spend much energy in timing control) [63]. Devices signals arriving earlier than expected cause much less degradation in **UFMC** than in **OFDM**.

UFMC (successfully demonstrated in [59] in an uplink scenario) can be considered as a potential candidate for future **5G** wireless systems which will have to support **IoT** and **Massive Machine Communication (MMC)**.

⁶**UFMC** provides higher spectral efficiency compared to **OFDM** due to the absence of **CP** [59]

2.2.5 Generalized Frequency Division Multiplexing

Since the first generation of mobile communication systems, the requirements for new generations that have come include higher data rates [18], [63]. But for 5G there is a paradigm shift: the main scenarios are *MTC* [63], *Tactile Internet* [19], and *Wireless Regional Area Network (WRAN)* [54]. As we have seen earlier, *OFDM* used in 4G can only address the challenges presented by these scenarios in limited way.

A flexible multicarrier modulation scheme, named *GFDM* has been proposed for the air interface of 5G networks. The flexibility of this technique allows it to cover *CP-OFDM* and *SC-FDE* as special cases [38]. *GFDM* is based on the modulation of independent blocks, where each block consist of a number of subcarriers and subsymbols [38]. The subcarriers are filtered with a prototype filter that is circularly shifted in time and frequency domain [38]. This process reduces the *Out-Of-Bound (OOB)* emissions, making fragmented spectrum and dynamic spectrum allocation feasible without severe interference with incumbent services or other users [38].

GFDM is a promising solution for the 5G PHY layer because its flexibility can address the different requirements. Since *GFDM* is confined in a block structure of $M K$ samples, where K subcarriers carry M subsymbols each, it is possible to design the time-frequency structure to match the time constraints of low latency applications [38].

In a *GFDM* block, the overhead is kept small by adding a single *CP* for an entire block that contains multiple subsymbols. This benefit in *GFDM* can be used to improve the spectral efficiency of the system or it can be traded for an additional *cyclic suffix (CS)*, that allows to relax the synchronization requirements of multiple users in an *MTC* scenario [38], [63]. In Fig. 2.8 we can see a comparision between the *CP* used in *GFDM* and *OFDM*. All synchronization algorithms developed for *OFDM* can be adapted for *GFDM* [38].

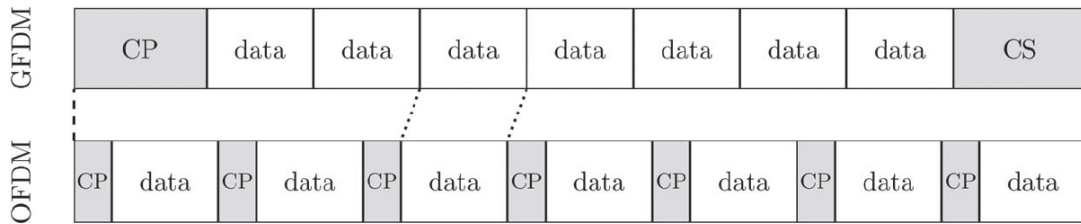


Figure 2.8: GFDM and OFDM frame Comparision for the MTC scenario [38]

2.2.5.1 System Description and Properties

Consider Fig. 2.9 where the block diagram of a *GFDM* transceiver is depicted. The binary data vector \vec{b} is provided by a data source, and is encoded to obtain \vec{b}_c . A mapper maps the encoded bits to symbols. The resulting vector \vec{d} denotes a data block that contains N

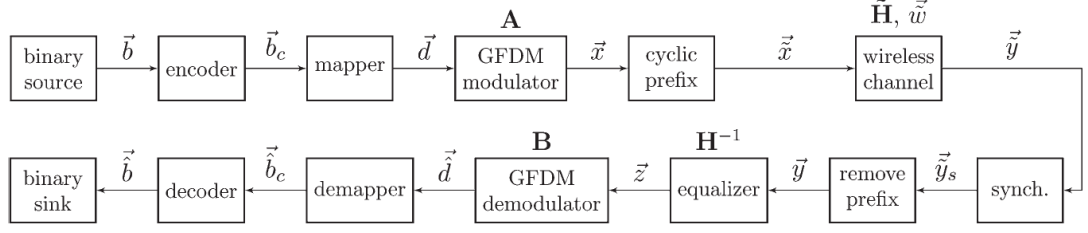


Figure 2.9: Block diagram of the transceiver [38]

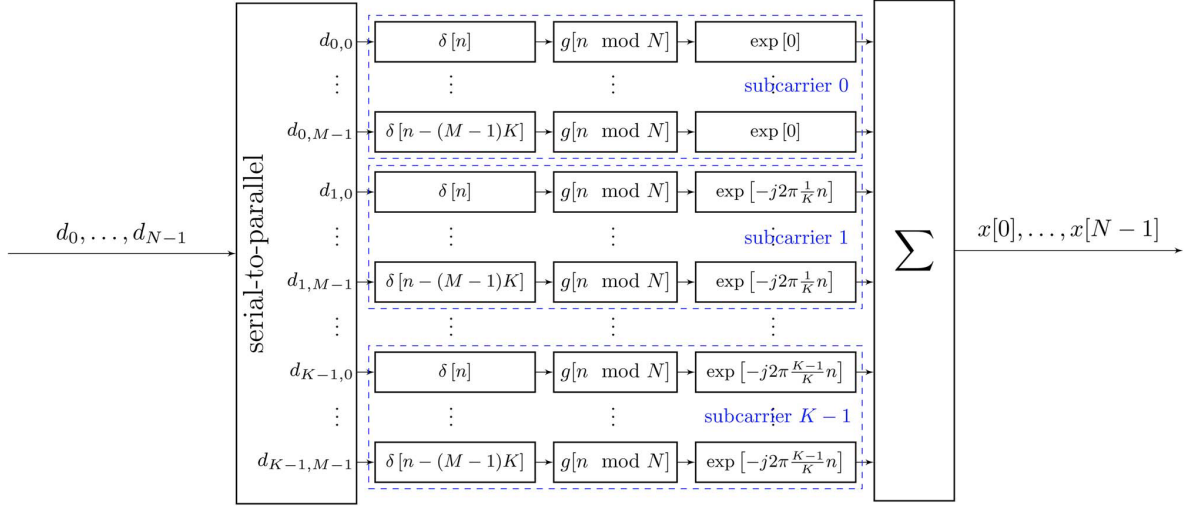


Figure 2.10: Details of the GFDM modulator [38]

elements, which can be decomposed into K subcarriers with M subsymbols each according to $\vec{d} = (\vec{d}_0^T, \dots, \vec{d}_{M-1}^T)^T$ and $\vec{d}_m = (d_{0,m}, \dots, d_{K-1,m})^T$. The total number of symbols N is given by $N = KM$. The individual elements $d_{k,m}$ correspond to the data transmitted on the k th subcarrier and in the m th subsymbol of the block. In Fig. 2.10 the GFDM modulator details are shown. Each $d_{k,m}$ is transmitted with the corresponding pulse shape [38]

$$g_{k,m}[n] = g[(n - mK) \bmod N] e^{-j2\pi \frac{k}{K} n}, \quad (2.24)$$

with n denoting the sampling index. Each $g_{k,m}[n]$ is a time and frequency shifted version of a prototype filter $g[n]$. The transmit samples $\vec{x} = (x[n])^T$ are obtained by superposition of all transmit symbols [38]

$$x[n] = \sum_{k=0}^{K-1} \sum_{m=0}^{M-1} g_{k,m}[n] d_{k,m}, \quad n = 0, \dots, N-1 \quad (2.25)$$

From 2.25, a linear mapping of \vec{d} containing KM data symbols to \vec{x} containing NM transmit samples according to [38]

$$\vec{x} = \mathbf{A} \vec{d}, \quad (2.26)$$

where \mathbf{A} is a $KM \times KM$ transmitter matrix with a structure according to [38]

$$\mathbf{A} = (\vec{g}_{0,0} \dots \vec{g}_{K-1,0} \vec{g}_{0,1} \dots \vec{g}_{K-1,M-1}). \quad (2.27)$$

Lastly, on the transmitter side a **CP** of N_{cp} symbols is added to produce \vec{x} .

To take into account the effect of the wireless channel, the model

$$\vec{y} = \mathbf{H}\vec{x} + \vec{w}, \quad (2.28)$$

is considered [38]. Therein \vec{y} is a vector containing the unequalized time samples at the receiver, $\vec{w} \sim \mathcal{N}(0, \sigma^2)$ is a vector of white Gaussian noise samples with variance σ^2 , and \mathbf{H} is a circular channel matrix that is built from an exponential power delay profile which denotes a Rayleigh multi-path channel. This allows employing zero-forcing channel equalization as is efficiently used in **OFDM** [38]. Introducing $\vec{z} = \mathbf{H}^{-1}\mathbf{H}\mathbf{A}\vec{d} + \mathbf{H}^{-1}\vec{w}$ as the received signal after channel equalization, the linear demodulation of the signal can be expressed as [38]

$$\vec{d} = \mathbf{B}\vec{z}, \quad (2.29)$$

where \mathbf{B} is a $KM \times KM$ receiver matrix. There are several receiver options for the **GFDM** demodulator:

- The *matched filter* (MF) receiver where $\mathbf{B}_{MF} = \mathbf{A}^H$, maximizes the **signal-to-noise ratio (SNR)** per subcarrier, but with the effect of introducing self-interference when a non-orthogonal transmit pulse is applied [38].
- The *zero forcing* (ZF) receiver $\mathbf{B}_{ZF} = \mathbf{A}^{-1}$ completely removes any self-interference at the cost of enhancing the noise [38].
- The linear *minimum mean square error* (MMSE) receiver $\mathbf{B}_{MMSE} = (\mathbf{R}_w^2 + \mathbf{A}^H \mathbf{H}^H \mathbf{H} \mathbf{A})^{-1} \mathbf{A}^H \mathbf{H}^H$ makes a trade-off between self-interference and noise enhancement [38]. \mathbf{R}_w^2 denotes the covariance matrix of the noise ⁷.

Finally, the received symbols \vec{d} are demapped to produce a sequence of received values \vec{b}_c , which are then passed to a decoder to obtain \vec{b} .

From this description of the transmitter and receiver, it can be concluded that **GFDM** is a type of filtered multicarrier system [38].

In [38] they successfully implemented a **GFDM** transceiver, proving that this system can be implemented with reasonable complexity using today's technology.

2.3 MAC Protocols for MTC communications

Until now we gave an overview of **PHY** layer techniques that are alternatives to **LTE-A**'s **OFDM** and could possibly fulfill the requirements of **MTC** in **5G**. But, in order to fully

⁷ In the case of MMSE reception, the channel is jointly equalized in the receiving process, hence the zero-forcing channel equalizer block is not required [38]

exploit the applications given by M2M communications, all layers in the network stack must provide adequate support in order to meet the service requirements. In this section we discuss existing MAC protocols that support MTC.

MAC protocols for supporting MTC must be designed with a set of requirements to satisfy the needs of the overlaying applications and scenarios [46]. We will now describe these requirements:

- *Data Throughput* - MAC protocols for MTC need to be highly efficient and present high throughput. Due to the limited channel/spectrum and the large number of devices accessing the channel, it is preferable that the MAC protocol minimizes the time wasted due to collisions or exchange of control messages [46]. The throughput has to be high in order to accommodate the very large number of devices [46].
- *Scalability* - MTC scenarios are expected to have a large number of nodes, and this number will only grow as the deployment of application scenarios with M2M communications becomes more prevalent [46]. Moreover, we have to take into account that the network conditions may be dynamic with nodes entering and leaving. Thus, it is imperative that the MAC protocol be easily scalable and adjusted gracefully to changing node densities with little or no control information exchange, and when new devices are added the fairness must be maintained [46].
- *Energy Efficiency* - This design requirement is one of the most important, in [46] three main factors are presented: 1) the fact that many of the devices in MTC networks are expected to be battery operated having then power constraints; 2) the economic impact of the power consumed by the communication structure; and 3) the environmental impact of the power consumed. Considering these factors, it is then very important that all operations associated with MTC be optimized to consume very low power [46]. Common methods to reduce MAC layer energy consumption include reducing the collisions, sleep scheduling, power control, and reducing idle listening [46].
- *Latency* - The network latency is a critical factor for many applications that rely on MTC. It is a factor that determines effectiveness and utility of the offered services [46]. In certain applications (e.g. real-time control of vehicles) it is extremely important to make the communication reliable and fast [46]. Also, even if a MAC protocol is throughput efficient, it has to ensure that all devices get equal chance to send their message [46]. It is worth noting that there are limitations to the amount of channel access latency that can be reduced, especially when the number of nodes increases [46].
- *Coexistence* - A significant fraction of the access networks for M2M communications is expected to operate in the unlicensed bands, since the spectrum costs associated with operating in licensed bands are reasonable [46]. With the increase of

the number of M2M devices, multiple M2M access networks will be deployed in close proximity and independently in the same unlicensed-based [46]. Due to this scenario, collisions due to hidden terminals from neighboring networks will occur, and this issue is addressed at the MAC layer [46].

- *Cost Effectiveness* - Devices involved in M2M communications must be cost effective so that it is affordable to deploy them. If the MAC protocol implemented in these devices has many desirable properties but relies on costly, complex hardware, then it is not practical. The MAC protocol should be designed to work effectively on simple hardware [46].

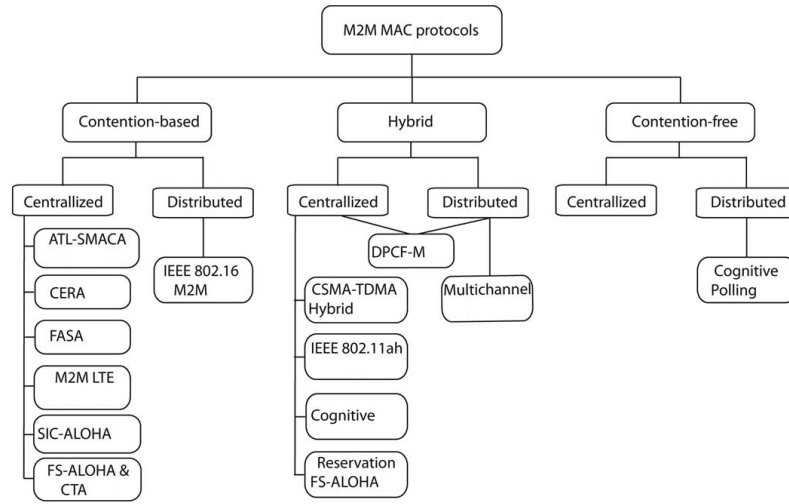


Figure 2.11: Taxonomy of M2M MAC protocols [46]

There are three types of MAC protocols: Contention-Based, Contention-Free, and Hybrid. A brief description of their characteristics will be given next.

Contention-Based MAC Protocols

Contention-based MAC protocols are simple to implement and setup. In these techniques, each node competes for the channel in various ways in order to acquire the channel and transmit data. The main disadvantage of these protocols is the lack of scalability [46], since the number of collisions, between concurrent transmission from different nodes, increases with the number of nodes. ALOHA and Carrier-Sense Multiple Access (CSMA)-based protocols are examples of Contention-based techniques.

Contention-based MAC protocols are largely unsuited for M2M communications due to the collisions which results in poor performance as the node density increases [46].

Contention-Free MAC protocols

Contention-free protocols preallocates transmission resources to the nodes in the network in order to eliminate the collisions issue. Classic examples of contention-free protocols are [Frequency Division Multiple Access \(FDMA\)](#), [Time Division Multiple Access \(TDMA\)](#) and [code division multiple access \(CDMA\)](#). In [FDMA](#), a fraction of the frequency bandwidth is allocated to each user all the time, whereas in [TDMA](#), the entire bandwidth is allocated to a user for a fraction of time [47] [52]. [CDMA](#) operates by assigning orthogonal codes to each user, which are then used to modulate the bit patterns [43] [61]. These are static contention free protocols where there are a fixed number of resources: times slots, frequency bands, and orthogonal codes that need to be assigned to the users. Such protocols have limited flexibility in the presence of dynamic network conditions and are not very efficient at low loads [46]. To solve these issues dynamic resource allocation methodologies are used.

The main advantage of contention-free protocols is their better channel utilization at high loads [46]. However, the utilization drops at low loads, the protocols are difficult to adapt when the number of nodes in the network varies, and usually have strict requirements on the hardware [46]. In a [M2M](#) communication context, the drawbacks outweigh the advantages and it is difficult for these techniques to provide the flexibility and scalability that is desired in these scenarios [46].

Dynamic contention-free protocols are better suited for networks with variability, since they dynamically adapt their operations as per the network conditions, these techniques require additional overheads that limit the overall improvement [46]. As example there are dynamic [TDMA](#) protocols. These techniques have stringent time synchronization requirements, which are difficult to implement, and result in extra bandwidth and energy consumption [46]. The average packet delays with these protocols are considerably higher, which is a concern for delay sensitive applications [46]. Finally, collisions may occur during certain stages of their operation, limiting their applicability in scenarios with high node density [46].

[CDMA](#)-based protocols are unsuitable for low-cost [M2M](#) devices primarily due to their complexity [46]. [CDMA](#)-based communication requires strict power control, this imposes computational and hardware requirements that increase the overall system cost [46]. Since [CDMA](#) requires computationally expensive operations for encoding and decoding messages, it is less appropriate for networks where devices lack special hardware and have limited computing power [46].

[FDMA](#) is the least suitable for operation with low-cost devices, compared to [TDMA](#) and [CDMA](#). One of the main reasons are that [FDMA](#) capable nodes require additional circuitry to communicate and switch between different radio channels [46]. Finally, [FDMA](#) has a strict linearity requirement on the medium that limits its practical use [46].

Hybrid [MAC](#) protocols

Contention-based protocols easily adapt to changing network scenarios and are better suited for networks with low loads. Contention-free protocols, on the other hand, eliminate collisions and have better channel utilization at higher loads. Hybrid protocols combine aspects of both these techniques in order to harness their advantages and disadvantages [46]. As an example we have hybrid MAC protocols that combine elements of CSMA with TDMA, FDMA and CDMA [46].

Hybrid protocols address some of the issues that arise with contention-based and contention-free protocols. Protocols that switch between random access-based operation at low loads and scheduled access at high loads avoid the degraded throughput and collisions of random access protocols [46]. These protocols are a promising approach for designing MAC protocols for M2M communications [46].

The main disadvantage of hybrid protocols that have been proposed in the context of wireless *ad hoc* and sensor networks is their scalability [46]. It is expected that the number of M2M nodes will exceed the number of nodes in currently deployed wireless networks. In this scenario, the incidence of collisions during the random access-based slot/code/frequency reservation stage of hybrid protocols becomes the reason that prevents the network from achieving high utilization [46].

Fig. 2.11 presents a taxonomy of existing M2M MAC protocols. In order to illustrate their main characteristics of existing M2M MAC protocols, the following subsections present a brief description of contention-based (Fast adaptive slotted ALOHA (FASA), Code Expanded Random Access (CERA), adaptive traffic load slotted MACA (ATL S-MACA) and M2M LTE) and hybrid protocols (distributed point coordination function-M (DPCF-M), CSMA-TDMA hybrid and IEEE 802.11ah).

2.3.1 DPCF-M

A hybrid MAC protocol for M2M communication named DPCF-M (proposed in [5]) addresses energy constrained M2M communication. This protocol uses IEEE 802.11's Carrier-Sense Multiple Access with collision avoidance (CSMA/CA) [30] and point coordination function (PCF) for channel access [46]. This protocol is designed for scenarios where there are two types of devices [46]: 1) local M2M nodes and 2) gateway-capable nodes. The latter are equipped with a short-range interface for local communication and a cellular radio interface, whereas M2M nodes are equipped with only a low-power short-range radio [46]. For local communication among neighboring nodes, the nonbeacon CSMA/CA mode of the IEEE 802.15.4 [46] is used. But when a M2M node needs to contact an external server using the cellular network, it uses one of the gateway-capable nodes to send data [46].

Fig. 2.12 shows the DPCF-M protocol operation. Device 1 is a M2M node and it wants to send data to an external server through the cellular link. The M2M device obtains access to the local channel using CSMA/CA, and then sends a request for gateway

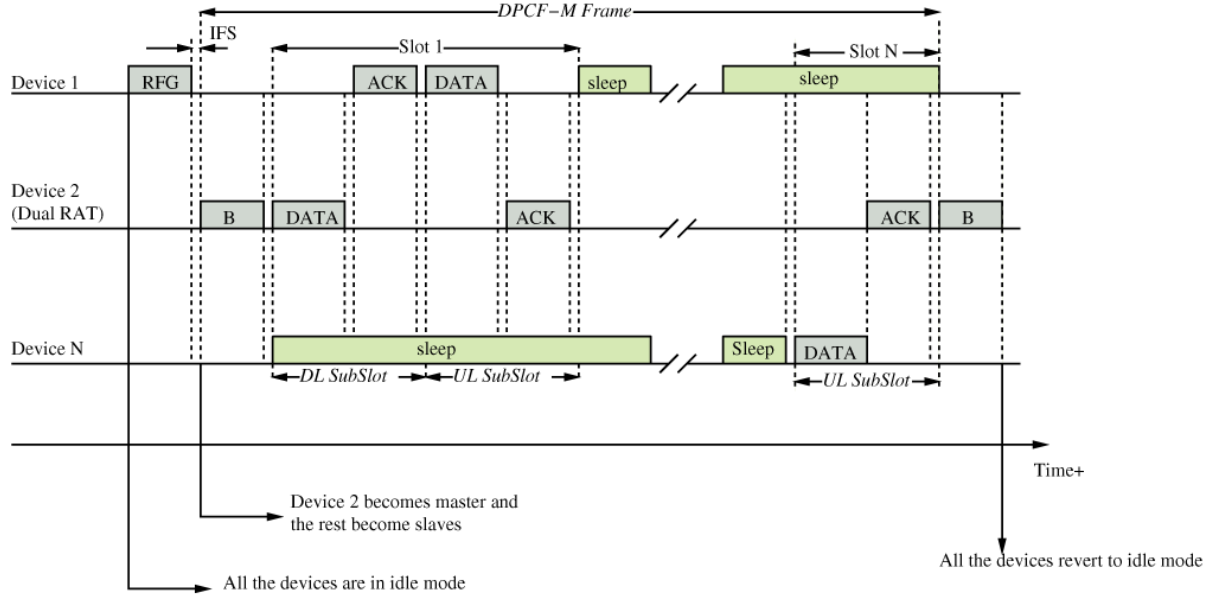


Figure 2.12: DPCF-M protocol frame structure [5]

(RFG) packet to its selected gateway (device 2). When device 2 receives the packet, it assumes the role of a master and starts a temporary cluster periodically transmitting a beacon during the existence of the cluster [46]. When devices overhear this beacon, they enter into the slave mode [46]. Devices in slave mode suspend their CSMA/CA-based operation and transmit only when the master permits [46]. Devices in the cluster are assigned individual slots by the master thereby allowing them to sleep at other times, and nodes that have no data to transmit, stay silent in their slots [46]. DPCF-M outperforms CSMA-based protocols in terms of the throughput and energy efficiency [46]. However, these advantages come with additional hardware costs for gateway nodes that require two radios [46]. Finally, the protocol does not eradicate the collisions that result during local communication using CSMA/CA [46].

2.3.2 Scalable Hybrid MAC

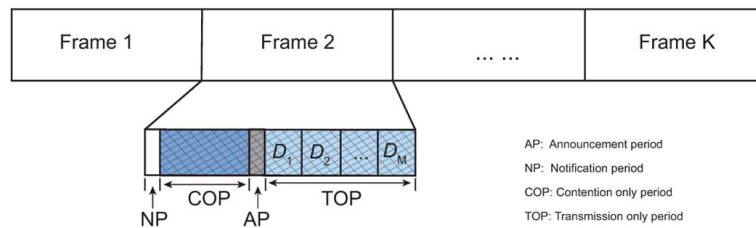


Figure 2.13: Frame structure for the contention-TDMA hybrid MAC protocol [34]

Liu [34] proposed a CSMA-TDMA hybrid MAC protocol for M2M communications. The protocol divides time in frames and each frame consists of four parts [46]: 1) notification period (NP); 2) contention only period (COP); 3) announcement period (AP); and 4) transmission only period (TOP), as shown in Fig. 2.13. The frame starts with a NP where the BS announces the start of the COP to all nodes. During the COP, nodes use p -persistent CSMA to send transmission requests to the BS [46]. Slots are allocated to successful nodes to transmit data in the TOP and the nodes are informed of their slots during the AP [46]. The BS solves an optimization problem to determine the optimum COP length and the number of devices that are allowed to transmit in the TOP [46]. The length of the contention period as well as the optimum contention probability for the p -persistent CSMA is communicated to all nodes by the BS during the NP [46]. While the protocol in [34] incurs into additional delays and energy consumption due to the time required for the COP and the need for contention, it provides a tradeoff between the performance between p -persistent CSMA and TDMA.

2.3.3 Adaptative Multichannel Protocol for large-Scale M2M

For a large scale M2M network, a FDMA hybrid MAC protocol based on the use of a common control channel is proposed in [29]. In this protocol, the available bandwidth is split into a number of channels, with one of them used as the control channel [46]. Time is divided into intervals of fixed length and each interval is further divided into three phases [46]: 1) estimation; 2) negotiation; and 3) data transmission. The estimation phase consists of a number of time slots in which nodes transmit busy tones on the common control channel if there is data to send or if they hear a busy tone from other nodes [46]. The number of active nodes is estimated statistically using a methodology that is based on the total number of busy tones sent and heard [46]. The negotiation phase consists of a number of slots, and nodes transmit data transmission requests, in the control channel, in each slot with a certain probability [46]. Nodes that receive request messages reply back confirming the channel to be used for the data transfer. The estimated number of active nodes dictates the length of the negotiation phase and the access probability [46]. Data transmission phase is where the nodes that have successfully reserved a channel with their receiver in the negotiation phases proceed to transmit their data. This protocol performs well in terms of channel utilization, but it adds an extra overhead due to the estimation phase [46].

2.3.4 Adaptative Traffic Load Slotted MACA

An extension of the slotted multiple access with collision avoidance (MACA) protocol called ATL S-MACA was proposed in [27] when carrier-sensing is not possible due to the inability of M2M nodes. This protocol slightly modifies the basic RTS-CTS-DATA-ACK-based scheme of MACA and RTS contention is adaptively controlled based on an estimate of the traffic load [46]. The idea that originated ATL S-MACA is the observation

that slotted **MACA** reaches its maximum throughput at some value of traffic load G_{opt} and then decreases rapidly [46]. The **BS** in **ATL S-MACA** estimates the traffic load G and then assigns a probability of G_{opt}/G to each node for RTS contention, keeping the offered traffic load constant at G_{opt} [46]. Since all nodes are allowed to send RTS packets at the beginning of a slot, **ATL S-MACA** suffers from increased number of collisions [46].

2.3.5 Code Expanded Random Access

CERA protocol is proposed in [45], and is based on a modification of the dynamic **random access channel (RACH)** resource allocation used in **LTE**. The goal of the proposed protocol is to provide support for a larger number of devices as compared to **LTE**, without increasing the resource requirements [46]. Random access in **LTE** is performed by nodes selecting one of the available orthogonal preambles and then sending it over a randomly selected subframe. As shown in Fig. 2.14(a), when a node wants to perform random access, it chooses one of the available preambles (denoted by A and B) and then selects a random access subframe (denoted by 1 and 2) to transmit the chosen preamble. In Fig. 2.14(a), the first user equipment, UE_1/G selects preamble B and transmits it in subframe 1. When two or more UEs select the same preamble and same subframe an collision occurs, as depicted in the second subframe presented in Fig. 2.14(a). Fig. 2.14(c) depicts the preambles as received by the **BS** in each subframe, in order to detect the different nodes sending requests. In [45], they present a modified access procedure, where a

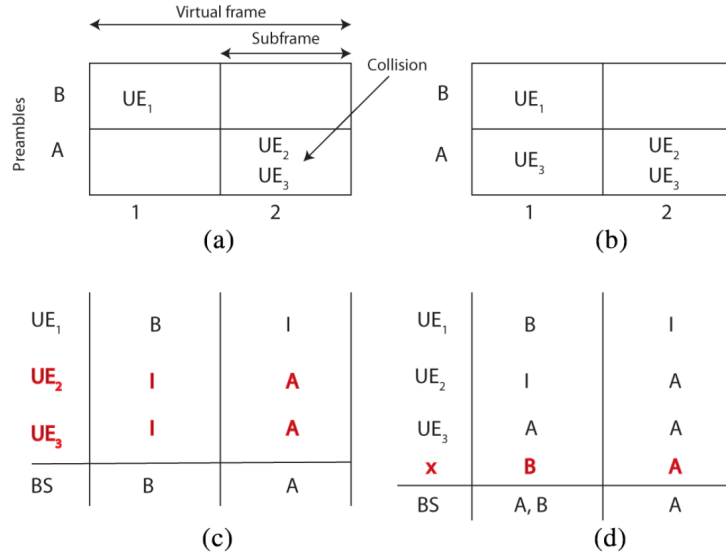


Figure 2.14: Code expanded random access [45]. (a) Current random access in LTE. (b) Code expanded random access. (c) Current LTE random access codewords, with collision for nodes 2 and 3. (d) Code expanded codewords, with phantom codeword in last row. I denotes a node is idle.

fixed number of subframes are grouped in a virtual frame. As shown in Fig. 2.14(b), two

subframes forms one virtual frame and there are three possible preambles that can be sent: A, B, and Idle(I). In the proposed protocol, instead of sending a preamble in a single subframe as in conventional LTE, nodes send a preamble in each of the subframes in a virtual frame [46]. The sequence of preambles transmitted by a node in a virtual frame constitutes its codeword and this is used by the BS to identify the node. This increases the number of contention resources and reduces the probability of collision (collision occurs when two or more nodes select the same codeword) [46]. Fig. 2.14(b) and (d) depicts the operation of this protocol. In this example, UE_1 , UE_2 , and UE_3 's codewords are formed by two preambles each (BI, IA, and AA, respectively) distributed over two subframes. Consequently, when the BS receives preambles A and B in the first subframe and preamble A in the second subframe, all possible permutations of the codewords that could have been sent are listed (AA, BA, AI, IA and BI) and it is assumed that all nodes that correspond to these codewords have transmitted. This leads to "phantom" codewords (BA and AI) indicated by an "x" in Fig. 2.14(d), that causes the BS to incorrectly add nodes that have not transmitted any codewords [46]. The probability of phantom codewords is reduced when the traffic load is high [46].

2.3.6 Enhancement of IEEE 802.11ah for M2M Communications

IEEE 802.11ah wireless protocol is expected to have the capability to support M2M communication [46]. To facilitate the transmission of this type of traffic, IEEE 802.11ah uses beacons to divide time into frames and each frame is further divided into two sections [46]: 1) restricted access window (RAW) and 2) offload traffic. Each RAW is divided into slots and a slot may either be allocated to a device by the access point (AP) or may be randomly selected by a device [46]. Within each slot selected by a device, in order to send a polling frame to request channel access, a binary exponential backoff-based access method is used. In [42] an enhancement is proposed to address the problem of estimating the required length of the RAW in order to facilitate the efficient channel access by devices [46]. The enhancement proposed divides the RAW into two sections: RAW uplink (RAW-UL) and RAW downlink (RAW-DL) with the uplink being the focus [46]. In order to determine the RAW-UL size, the AP first determines the number of devices wishing to transmit. The AP uses the probability of successful transmissions in the last frame to estimate the number of devices. The number of slots in the RAW-UL is a linear function of the estimated number of active nodes [46]. This proposed enhancement achieves a higher probability of successful transmission compared to the original IEEE 802.11ah protocol [46].

2.3.7 Fast Adaptive Slotted ALOHA

The FASA protocol [62] is proposed for random access in event-driven M2M communications. In this protocol, the number of backlogged devices N_t is estimated by using drift analysis on the access results of the past slots [46]. Each node, using this network

information, is then assigned to a slot with a transmission probability of $1/N_t$. The BS is responsible for estimating the number of backlogged nodes and communicating the transmission probability to backlogged devices [46].

2.3.8 LTE-A MAC layer design for MTC

The MAC layer design for M2M communication in LTE-A is presented in [12]. In this article they argue that the overhead associated with the signaling required for the RRC mechanism used in LTE is prohibitive in a case such as MTC where devices may have very little data to send. In order to make the channel access mechanism more efficient, they propose a new policy where backlogged nodes first send an access request to the BS using a preamble. When the BS receives the preamble, it allocates uplink resources to the node to send the RRC setup request. In this case, the nodes directly send data in the form of a MAC PDU, instead of sending a RRC setup request as in LTE-A. The BS is modified to recognize the MAC PDU, which may contain the node identity and security information [46]. Another enhancement is proposed by the authors where the MAC protocol is further simplified by allowing nodes to directly send the data in encoded format along with a special preamble. This proposed simplifications to the MAC layer in LTE-A improve the efficiency and avoid unnecessary control overhead [46].

Lo *et al* address the overload problem during random access of physical random access channel (PRACH) in LTE-A due to simultaneous transmissions by a large number of M2M devices. 3GPP has proposed solutions for the PRACH overload problem, but these methods do not address the issue of PRACH overload detection and notification [46]. So, [3] propose a self-optimizing overload control (SOOC) mechanism, which dynamically detects congestion in a PRACH channel. In the proposed mechanism, M2M devices count the number of times they do not receive a response from the BS to their random access requests [46]. The BS, in order to adapt to the overload, increases the number of slots for PRACH depending on the value of the received PRACH overload indicator. The increase or decrease in the PRACH random access slots may be done in the FD, TD, or both [46]. When the end of a random access cycle is reached, the BS first estimates the collision probability p_c in the cell or sector using the PRACH overload indicators [46]. This probability is then used to calculate the number of random access requests per second B using $B = -L \ln(1 - p_c)$ where L is the current number of random access resources (i.e. slots) per second. Then, using the desired collision probability p'_c and the current estimate of B , the BS calculates the required number of random access slots per second L' using $B = L' \ln(1 - p'_c)$. The additional random access resources required are then determined by the BS as $L' - L$.

2.3.9 M2M MAC protocols overview

In Table 2.1 we can see a comparison between the protocols presented in the previous subsections. It is worth noticing that current mobile network(LTE) techniques are costly

and do not scale well, which does not meet the requirements for **M2M MAC** presented earlier.

Table 2.1: Comparison of MAC protocols specific to M2M communication

Protocol	Through-put/utiliza-tion	Scalabil-ity	Energy efficiency	Latency	Cost	Burst han-dling
DPCF-M	Moderate	Moderate	Moderate	Moderate	Low	Yes
CSMA-TDMA hybrid	Moderate	Moderate	Moderate	Low	Low	No
Contention-FDMA hybrid	Moderate	Moderate	Low	High	Low	Yes
ATL S-MACA	Low	Low	Low	High	Low	No
CERA	High	Moderate	Moderate	Low	High	Yes
IEEE 802.11ah	High	High	Moderate	Moderate	Low	No
FASA	Low	Low	Low	High	Low	No
M2M LTE [12]	Moderate	Low	Moderate	Moderate	High	No
M2M LTE [3]	High	Moderate	Moderate	Moderate (1ms latency)	High	Yes

2.3.10 5GNOW Proposed MAC protocol

Wunder *et al* proposed in [63] a unified uplink frame structure. They defend that a **5G** approach must be able to efficiently support different traffic types, which all have to be part of future wireless cellular systems. Fig. 2.15 depicts their vision of a unified frame structure concept. Type I is the classical bit pipe traffic with high-volume data transmission and high-end spectral efficiency that exploits orthogonality and synchronism wherever is possible. This bit pipe may also be a real-time carrier. Vertical layering at common time-frequency resources generates a non-orthogonal signal format supporting heterogeneous cell structures and cell edge transmissions more efficiently [63]. For high-volume data applications in those cell areas (type II), a multi-cell multi-user transceiver concept is required.

Types III and IV are associated to sporadic asynchronous **MTC** traffic, possibly containing an energy-efficient spreading element ⁸, for example, for sensors in the case of type IV, as depicted by the green shade in Fig. 2.15.

⁸Weightless initiative (<http://www.weightless.org/>) has shown that, from an energy perspective, it is beneficial to stretch the transmission in time by spreading.

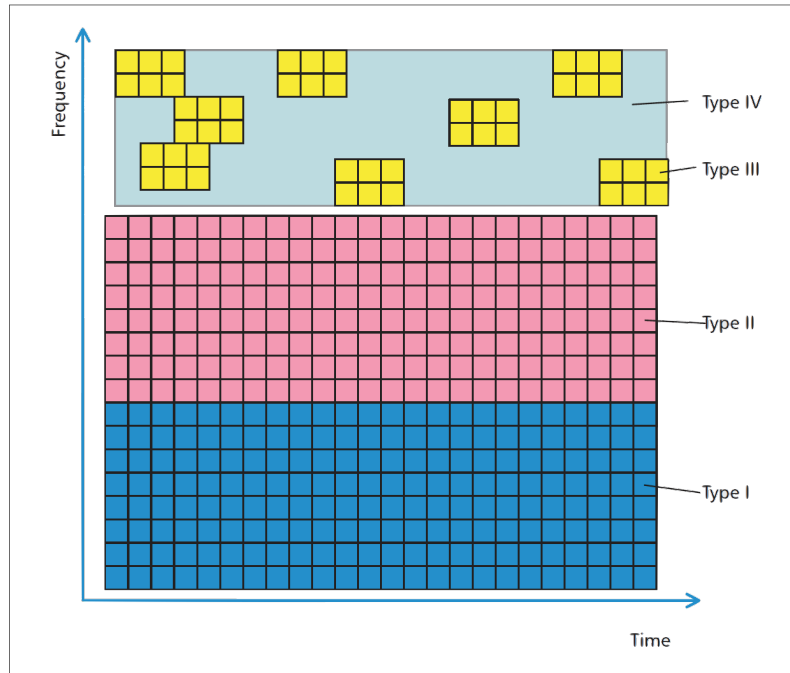


Figure 2.15: The 5G vision of a unified frame for different types of traffic [63].

An **IDMA**-like approach, is proposed as an appealing candidate to generate these different types of signal layers [63]. In Asynchronous **IDMA** scheme [44], users are distinguished by different chip-level interleaving methods instead of by different signatures as in a conventional **CDMA** system. Being a wideband scheme, **IDMA** inherits many advantages from **CDMA**, in particular, diversity against fading and mitigation of other-cell user interference [44]. One of the special benefits of **IDMA** is that it allows a very simple (and near-optimal) chip-by-chip iterative multiuser detection strategy [44]. Such low complexity and high performance attributes can be maintained in a multipath environment [44].

In order to correctly solve collisions, this **MTC** protocol needs to know in advance the number of transmitting nodes. Another disadvantage, that is also valid for **CDMA** protocols, is that **IDMA** only works successfully when it is able to assign orthogonal codes to each node. This comes as a limitation in densely populated networks.

2.4 Multipacket Reception

In a conventional communication system, receivers can only receive a packet from each source at a time. These systems are classified as **single packet reception (SPR)**. On the contrary, **MPR** systems are capable of simultaneous decoding of multiple packets from more than one concurrent transmission. In these systems, even if a collision occurs, it is possible to decode the packets that were transmitted [35]. Fig. 2.16 depicts the taxonomy of **MPR** techniques. These techniques are divided in three main classes, which corresponds to the place where the responsibility of enabling **MPR** lies. This classification

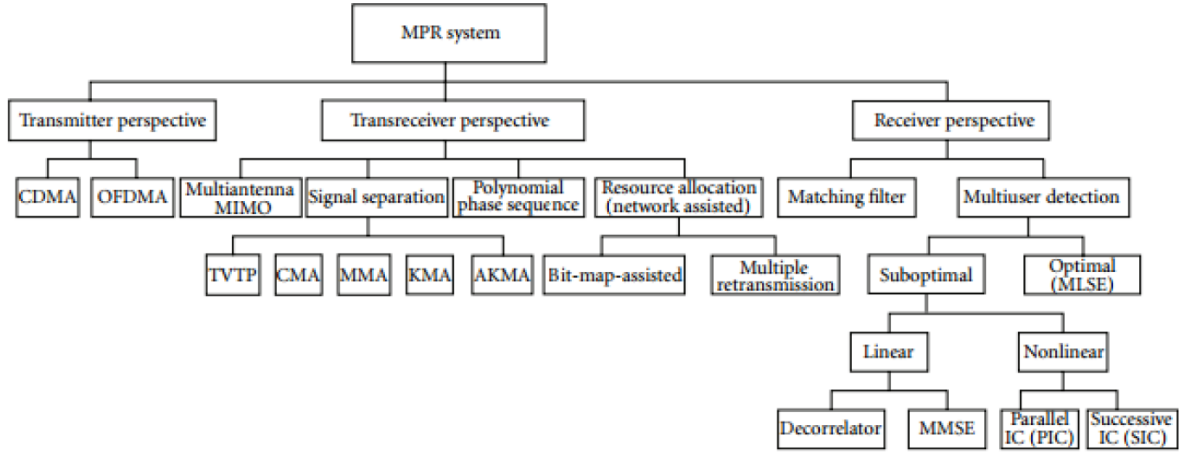


Figure 2.16: Classification of techniques applied for MPR [35]

is given based on three perspectives:

- *Receiver perspective* - Techniques used in this class shift the responsibility from the transmitters to the receivers [35].
- *Transmitter perspective* - This set of techniques require a significant effort by the transmitter [35]. The basic idea of techniques that fall in this class is to separate the different signals into orthogonal signaling dimensions, thus allowing multiple users to share the same channel. [FDMA](#), [CDMA](#) and [OFDMA](#) (all described in previous sections) are examples of this class.
- *Transceiver perspective* - The [MPR](#) in this class of techniques is enabled by the cooperation, on some operations, between receivers and transmitters.

A brief description of some of the techniques that fall on the classes presented above is given in following subsections. It starts by describing receiver techniques like [MIMO](#), [Network-assisted Diversity Multiple Access \(NDMA\)](#), [Successive Interference Cancellation \(SIC\)](#), and [Hybrid automatic repeat request Network Diversity Multiple Access \(H-NDMA\)](#), which is an hybrid solution, i.e. a design that uses more than one of the techniques classified above. Finally, it presents two proposed [Non-Orthogonal Multiple Access \(NOMA\)](#) techniques.

2.4.1 MIMO

An multi-antenna [MIMO](#) system [33] achieves [MPR](#) by exploiting the spatial diversity of the transmissions. In these systems, each antenna corresponds to a different channel characteristic $H(t)$ [35]. Channel detectors can easily distinguish packets sent through different antennas. In order to implement [MPR](#) in a multi-antenna [MIMO](#) system, both the transmitters and receivers have to implement specific functionalities [35].

2.4.2 Network Diversity Multiple Access

NDMA [56] relies on storing collided packets in memory instead of discarding them. They are later combined with future retransmissions in order to extract all the collided information packets. This technique uses *diversity combining* ideas in order to separate the collided packets. However, it defers from traditional diversity techniques since the required diversity is not created through multiple receiving antennas [56]. As in **CDMA**, network resources are used to provide diversity through selective retransmissions. The main advantage of **NDMA** is that no channel slot is lost when a collision takes place [56]. If k users collide, only k time slots are required to resolve the collision and successfully forward the k information packets. Since this is the same number of slots required if there were no collisions, **NDMA** introduces no throughput penalties [56]. It is mandatory that all users in the system possess a unique orthogonal identification. This requirement causes bandwidth inefficiency, especially with large user populations [56]. Another disadvantage of **NDMA** is its inability to cope with a low **SNR** scenario, where packet separation may not be possible due to noise interference [23].

2.4.3 Successive Interference Cancellation

In **SIC**, the multi-users's signals are demodulated and canceled from the strongest to the weakest according to their received signal power [56]. It is then required that the signals' power received at a given node have enough separation between them. **SIC** has been shown to improve bandwidth utilization in cellular networks [4].

A low complexity **SIC-GFDM** receiver was implemented in [26]. It was shown that, for high-order **QAM** signaling, the error performance can be significantly improved with **SIC** at reasonable computational cost.

2.4.4 Hybrid automatic repeat request network division multiple access

H-NDMA was first introduced in [23] and extended in [24]. This protocols uses cross-layered architecture to implement a slotted random access protocol with gated access. [24] considers a scenario where terminals are low resource battery operated devices, whereas the **BS** is a high resource device that runs the **MPR** with **hybrid ARQ (H-ARQ)** error control in real-time. **H-NDMA**, in comparison to **NDMA**, adds additional retransmissions, for the packets that failed after an initial set of **NDMA**'s k transmissions, for k colliding users. **H-NDMA** is **NDMA** protocol that uses **H-ARQ** concepts and adapts to lower **SNR** scenarios. **H-NDMA** may use less transmissions than k but only if the receiver is capable of separating the collided signals with less transmissions.

Fig. 2.17 depicts a **H-NDMA** reception scheme, with two **Mobile Terminal (MT)**s transmitting. In this scenario, the **MTs** contend for the uplink channel by transmitting data right after receiving the **SYNC** packet from the **BS**. If the **BS** does not detect any collision till the end of each slot, it broadcasts a **SYNC** to signal the beginning of the next

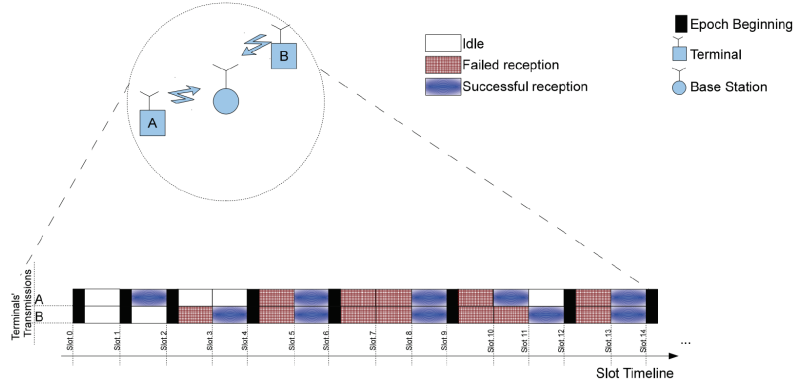


Figure 2.17: H-NDMA MPR scheme [24]

epoch; on the other hand, if a collision is detected, the BS broadcasts an ACK to signal which terminals should retransmit [24]. The epoch only ends when all data packets are correctly received or when the maximum number of retransmissions is reached, i.e. after $P + R$ where P is the number of MTs that collided and R is the maximum number of H-ARQ retransmission slots.

Ganhão *et al* [24] evaluated the performance of H-NDMA for the SC-FDE receiver, and the obtained results show that H-NDMA improves the network capacity, and reduces the packet delay and the energy consumption when compared to the basic NDMA MAC protocol, or to the classical H-ARQ protocol. They also concluded that mis-detection and false-alarm errors causes a slight degradation in performance.

One disadvantage of H-NDMA is the strict synchronization in time, so that the terminals can identify the epoch beginning.

2.4.5 Non-Orthogonal multiple access

NOMA is a multiple access technique where all the users can use resources simultaneously. This scenario leads to inter-user interference. Thus, more complicated Multi-User Detection (MUD) techniques are required to retrieve the users' signals at the receiver [2]. NOMA techniques superposes multiple users in the power domain so that its user separation can be achieved through SIC and capacity-achieving channel codes such as the Turbo code and low-density parity check [48]. CDMA and IDMA are examples of NOMA techniques.

A NOMA technique using SIC is proposed in [48]. It adopts a SIC receiver as a baseline receiver scheme for robust multiple access. They demonstrated that the downlink NOMA with SIC improves the capacity and cell-edge user throughput performance based on wideband channel quality indicator (CQI) without relying on the availability of the frequency-selective CQI at the BS transmitter side.

Since, in the uplink, Orthogonal Multiple Access (OMA) (e.g. OFDMA) is not optimal in terms of spectral efficiency and cannot achieve the system upper bound, Al-Imari *et*

al [2] defend that to improve the system spectral efficiency, NOMA techniques needs to be adopted in next generation of wireless networks.

Al-Imari *et al* [2] proposed an uplink NOMA for OFDM without coding/spreading redundancy. In this technique the users uses subcarriers without any exclusivity, and at the receiver, optimum MUD is implemented for users' separation [2]. The main advantages of the proposed NOMA scheme are [2]:

1. Higher spectral efficiency comparing to current OMA and NOMA techniques.
2. Lower receiver complexity comparing to optimal unconstrained NOMA scheme.

The proposed NOMA technique in [2] significantly improves the system spectral efficiency and fairness comparing to OMA. Despite the inter-user interference, the NOMA technique proposed in [2] achieves a link-level performance that is very close to the single-user case. However, NOMA also has requirements that limit its use in asynchronous uncoordinated scenarios: as an example, the signal power level separation needed by SIC requires synchronization.

MULTIPACKET RECEPTION

3.1 Introduction

This chapter starts by describing the cellular network where the BS runs a MPR receiver. Secondly, it presents two analytical models: the first one, proposed in [22], for H-NDMA performance described in section 2.4.4, and finally a simplified model which takes into account that, on large systems, H-NDMA performance approaches the CDMA's. Considering up until two power levels, the optimum gap between the power levels and the minimum E_b/N_0 for the levels are evaluated. Lastly, a comparison is made between the two presented models.

3.2 System Characterization

This dissertation considers a structured wireless system where a set of MTs send data to a BS using a slotted data channel. MTs are low resource battery operated MTC devices, whereas the BS is a high resource device that can use [Diversity Combining \(DC\)](#) to cope with packet errors due to poor propagation conditions or [Multi-Packet Detection \(MPD\)](#) due to collisions. The BS can also employ hybrid techniques that combine DC and MPD. The MTs send data packets on time slots defined by the BS, that also controls the transmission power. Perfect channel estimation and synchronization is assumed. Colliding packets on each slots are also assumed to arrive simultaneously, which means that perfect time advance mechanisms exist to compensate different propagation times, making the offsets below the CP duration time.

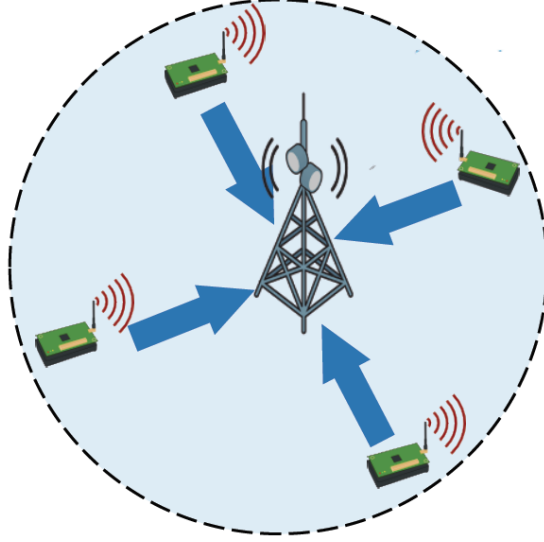


Figure 3.1: System Model

3.2.1 Multipacket detection receiver performance

SC-FDMA is considered for the system's uplink, based on the uncoded [Iterative Block DFE \(IBDFE\)](#) MPR receiver from [22] for an [Offset Quadrature Phase Shift Keying \(OQPSK\)](#) constellation. Using an [IBDFE](#) technique that performs [SIC](#) for each iteration, it allows the reception of more than one packet per slot in average [9]. The analytical expression for the Packet Error Rate (PER) in [22] is presented in this section.

3.2.1.1 Multipacket detection receiver

A data block of N symbols transmitted by a MT p can be expressed in the time domain as $\{s_{n,p}; n = 0, \dots, N-1\}$, and on the frequency domain as $\{S_{k,p}; k = 0, \dots, N-1\}$. At the BS, the received signal from P MTs for a given transmission l is expressed in the frequency domain as $Y_k^{(l)} = \sum_{p=1}^P S_{k,p} H_{k,p}^{(l)} + N_k^{(l)}$, where $H_{k,p}^{(l)}$ is the channel response for the p th MT at the l th transmission and $N_k^{(l)}$ is the background noise for the l th transmission, modelled by a null average Gaussian random variable with variance $\sigma_{N^{(l)}}^2$.

For P MTs that transmit through L channels (e.g. L transmissions on a single antenna, or using m transmissions received by L/m uncorrelated receiver's antennas), the received L transmissions are characterized as $\mathbf{Y}_k = [Y_k^{(1)}, \dots, Y_k^{(L)}]^T$, where $\mathbf{H}_k^T = [\mathbf{H}_{k,1}, \dots, \mathbf{H}_{k,P}]$ and $\mathbf{H}_{k,p}^T = [H_{k,p}^{(1)}, \dots, H_{k,p}^{(L)}]$ for $p = [1, \dots, P]$, $\mathbf{S}_k = [S_{k,1}, \dots, S_{k,P}]^T$, and $\mathbf{N}_k^T = [N_k^{(1)}, \dots, N_k^{(L)}]$, where T represents the transpose of a matrix. So

$$\mathbf{Y}_k = \mathbf{H}_k^T \mathbf{S}_k + \mathbf{N}_k \quad (3.1)$$

The expanded version of \mathbf{Y}_k is

$$\begin{bmatrix} Y_k^{(1)} \\ \vdots \\ Y_k^{(L)} \end{bmatrix} = \begin{bmatrix} H_{k,1}^{(1)} & \dots & H_{k,P}^{(1)} \\ \vdots & \ddots & \vdots \\ H_{k,1}^{(L)} & \dots & H_{k,P}^{(L)} \end{bmatrix} \begin{bmatrix} S_{k,1} \\ \vdots \\ S_{k,P} \end{bmatrix} + \begin{bmatrix} N_k^{(1)} \\ \vdots \\ N_k^{(L)} \end{bmatrix}. \quad (3.2)$$

If, for a given transmission l , a MT p has an attenuation gain, $|\xi_{l,p}|$, then $H_{k,p}^{(l)}$ should be replaced by $|\xi_{l,p}|H_{k,p}^{(l)}$. In the occasion where the p th MT does not transmit for a given slot l then $H_{k,p}^{(l)} = 0$.

3.2.1.2 IBDFE design

In the IBDFE, both the feedforward and the feedback filters are implemented in the FD [9] [7]. The equalizer includes two parts: 1) the feedforward filter, which partially equalizes for the interference and 2) the feedback signal, which removes part of the residual interference [10]. The IB-DFE receiver [22] runs N_{iter} iterations using the L channels, from the strongest to the weakest received signal power, to detect each of the P MTs. The estimated data symbol, $\tilde{S}_{k,p}^{(i)}$, for a given iteration i and MT p is given by

$$\tilde{S}_{k,p}^{(i)} = \mathbf{F}_{k,p}^{(i)T} \mathbf{Y}_k - \mathbf{B}_{k,p}^{(i)T} \tilde{\mathbf{S}}_k^{(i-1)}, \quad (3.3)$$

where $\tilde{\mathbf{S}}_k^{(i-1)} = [\tilde{S}_{k,1}^{(i-1)}, \dots, \tilde{S}_{k,P}^{(i-1)}]^T$ denotes the soft decision estimates from the previous iteration for all MTs. $\mathbf{F}_{k,p}^{(i)T} = [F_{k,p}^{(i,1)}, \dots, F_{k,p}^{(i,L)}]$ are the feedforward coefficients,

$$F_{k,p}^{(i,l)} = \frac{H_{k,p}^{(l)*}}{\frac{\sigma_N^2}{\sigma_S^2} + \sum_{l=1}^L |H_{k,p}^{(l)}|^2}, \quad (3.4)$$

and $\mathbf{B}_{k,p}^{(i)T} = [B_{k,p}^{(i,1)}, \dots, B_{k,p}^{(i,P)}]$ are the feedback coefficients,

$$B_{k,p}^{(i)} = \sum_{l=1}^L F_{k,p}^{(i,l)} H_{k,p}^{(l)} - 1, \quad (3.5)$$

calculated in [22] to minimize the mean square error at the receiver.

The mean square error of MT p at the i th iteration [22] is

$$\sigma_p^{2(i)} = \frac{1}{N^2} \sum_{k=0}^{N-1} \mathbb{E} \left[\left| \tilde{S}_{k,p}^{(i)} - S_{k,p} \right|^2 \right]. \quad (3.6)$$

where $\mathbb{E} \left[\left| \tilde{S}_{k,p}^{(i)} - S_{k,p} \right|^2 \right]$ can be calculated using [22]. The Bit Error Rate (BER) of MT p at the i th iteration for a [Quadrature Phase Shift Keying \(QPSK\)](#) constellation is given by

$$BER_p^{(i)} \simeq Q \left(\frac{1}{\sigma_p^{(i)}} \right), \quad (3.7)$$

where $Q(x)$ denotes the Gaussian error function.

For an uncoded system with independent errors, the Packet Error Rate (PER) for a fixed packet size of M bits is

$$PER_p^{(i)} \simeq 1 - (1 - BER_p^{(i)})^M. \quad (3.8)$$

Equation (3.8) provides a generic function that can be used to calculate the PER for any system given the channel response \mathbf{H}_k and the bit energy to noise ratio (E_b/N_0) for the signal received from each MT. The energy received from MT p during transmission l to the BS is modelled by the $H_{k,p}^{(l)}$ coefficients, which account the attenuation gains and different transmission powers. When a MT does not transmit, the channel coefficient value is set to zero.

3.2.1.3 Approximate PER model

On a large system, H-NDMA performance approaches the code division multiple access (CDMA) with random spreading when independent channels are used [25]. Schemes like frequency shifting can also provide equivalent performance in equal channels.

It was proved [60] that, by combining successive cancellation and [minimum mean-square error \(MMSE\)](#) demodulation, any vertex of the Shannon capacity region of the [CDMA](#) channel can be achieved. Tse *et al* [57] showed that the SINR of the linear MMSE for a user n when the spreading length is N , with P competing MTs is given by

$$SINR_n = \frac{Q_n}{\sigma^2 + \frac{P}{N} \mathbb{E}[I(Q, Q_n, SINR_n)]}, \quad (3.9)$$

where $I(Q, Q_n, SINR_n)$ denotes the interference term for interferer n , for a power distribution Q , and is calculated using

$$I(Q, Q_n, SINR_n) = \frac{QQ_n}{Q_n + QSINR_n} \quad (3.10)$$

In a large system, the SIR is deterministic and approximately satisfies [57]

$$SINR_n \approx \frac{Q_n}{\sigma^2 + \frac{1}{N} \sum_{i=1, i \neq n}^P I(Q_i, Q_n, SINR_n)}. \quad (3.11)$$

where Q_i is the received power of user i . This results that for a large system, the total interference can be decoupled into a sum of the background noise and an interference term from each of the users [57]. Equation (3.9) can be used to estimate the SINR, which is equal to $2E_b/(N_0 + I)$ for QAM.

3.3 Accuracy Analysis

This section analyses the accuracy of the PER models described in this chapter for the MPR receiver, validating them using simulation. A SC-FDE modulation is considered

with an FFT-block of $N=256$ data symbols, a cyclic prefix (CP) of 32 symbols, using a bandwidth of 64 MHz. The simulations were performed in MATLAB considering a frequency and time selective channel with 16 equal power rays, spread uniformly over the CP duration.

3.3.1 Packet error rate evaluation

The performance of the MPR receiver was analysed using a physical layer simulator implemented in Matlab. Figure 3.2 depicts the packet error ratio (PER) in function of the ratio of bit energy per noise (E_b/N_0), measured for a system with $P = 10$ MTs transmitting a packet $L = [1, 10]$ times, in a known channel, i.e. it is assumed that matrix H is known. The figure shows that the E_b/N_0 required to receive the 10 MTs decreases when more transmissions are combined, functioning as an adaptive code spreading approach. It also shows that the number of packet decoded is higher than the number of transmissions, given that it is capable of receiving the 10 packets requiring only 7 transmissions. This

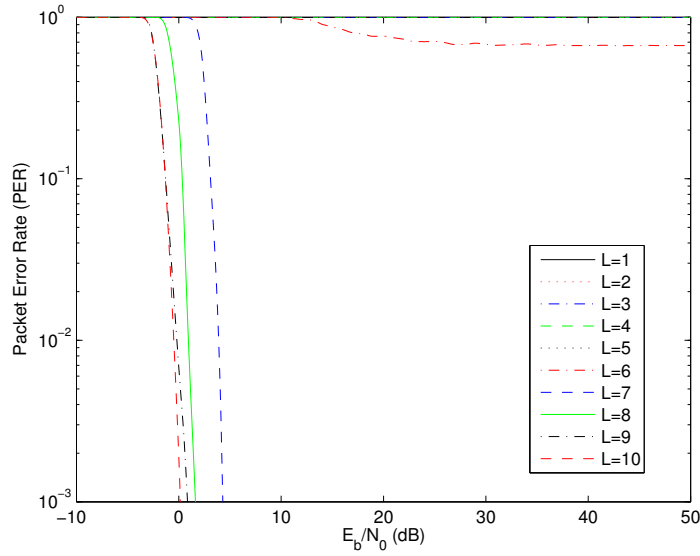


Figure 3.2: PER performance for $P=10$, $L=[1,10]$, and 4 iterations

receiver's performance can be summarized by the minimal E_b/N_0 value (at the receiver) above which the PER is below 10^{-3} . Figure 3.3 depicts these values for $P = \{1, 2, 4, 10\}$ MTs in function of the number of transmissions (L), considering one receiving power level ($N = 1$) and two power levels ($N = 2$), the higher (h) and the lower (l), separated by 12 dB, with MTs distributed evenly between the two power levels. The results show that for all combinations there are E_b/N_0 and L values above which the system is capable of successfully receiving the packets, with $L \leq P$. It also shows that with the offset of -12dB between power levels, the receiver using two levels requires much less transmissions for the same number of MTs and almost the same E_b/N_0 for the lowest power level, except for the lowest L value with a successful reception. For instance, for $P = 10$ MTs the number

of transmissions is reduced from 7 to 5, when $N = 2$ power levels are used, requiring almost 10 dB for $L=5$, but only 3dB for the E_b/N_0 of the lowest power with $L=6$. .

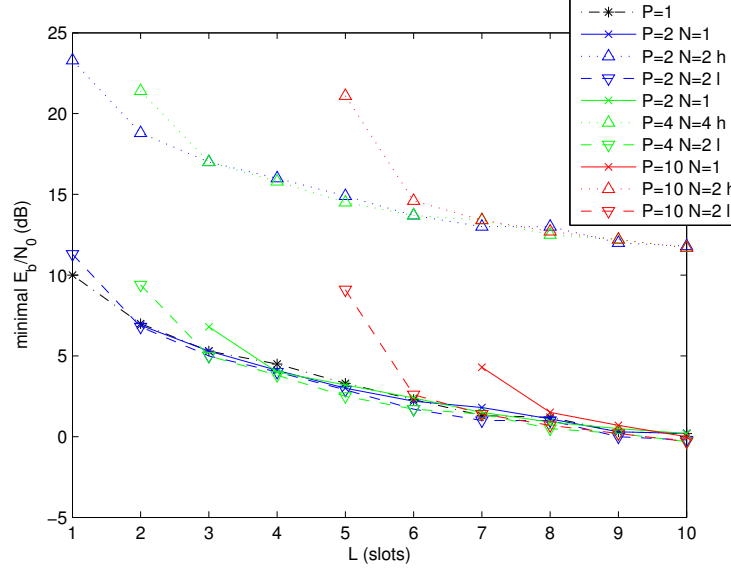


Figure 3.3: Minimum E_b/N_0 required to transmit successfully with one power level, $P=[1,10]$, $L=[1,10]$, and 4 iterations

3.3.1.1 Power separation

In order to enable MPR, the MTs signals received at the BS need to have different powers with enough separation between them to allow the serial resolution from the signal with the highest power to the one with lowest power. Figure 3.4 depicts the PER level curves when power diversity and two power levels are used. It shows that for the channel sample considered, it is possible to have an average PER below 10^{-3} with $L = 5$ for $E_b/N_0 > 10dB$ and for a power separation of 12dB. This shows that performance increases when power multiplexing is applied, reducing the ratio of the number of transmissions needed per number of packets received. When multiple power levels are used, the number of data slots required is conditioned by the power level with the maximum number of MTs, assuming that SIC can be used successfully.

3.3.2 Analytical model versus approximate model

The exact and approximate models were simulated using MATLAB in the conditions presented on section 3.3, for a total number of MTs $P=60$. Figure 3.5 depicts a comparison between simulated and estimated/approximate PER values in function of the number of slots used, for a number of MTs, transmitting with the upper power level, $q_2 = \{1, 24, 30\}$. The scenarios with $q_2 = \{24, 30\}$ are more likely to happen (i.e. a 60%-40% or 50%-50%) in terms of MTs distribution between the power levels, given that are more efficient, and

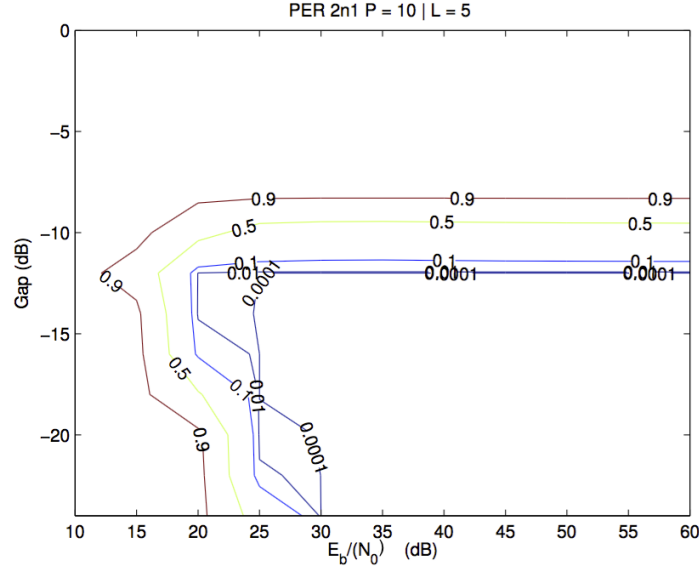


Figure 3.4: PER performance for E_b/N_0 and power offset for $P=10$, $L=5$

are more probable when random selection of power level is used. The figure clearly shows that the estimated model presents a good approximation of the one obtained with simulated PERs, in the case where $q_2 = 24$ both models results overlap. On the other hand, for $q_2 = 1$, the models show a visible deviation, which results from not considering in the model the power diversity already present in the channels from the different MTs.

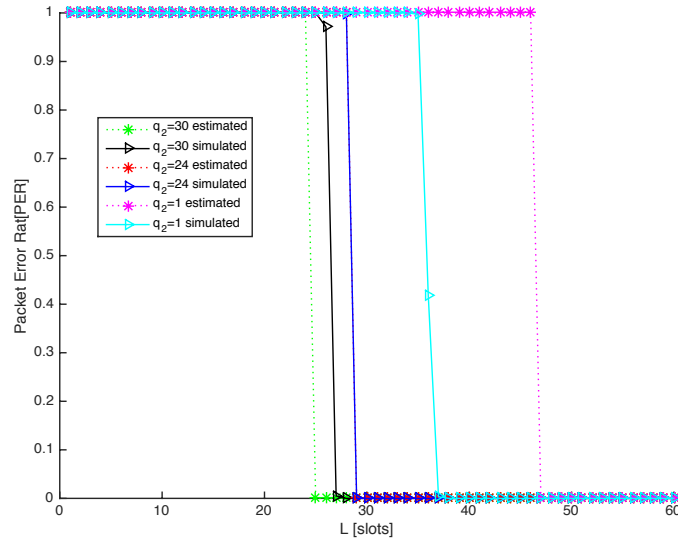


Figure 3.5: Estimated and simulated PER performances comparison for different number of MTs using the upper transmission level q_2

Another way to compare the performance of both models, would be to evaluate the

average number of transmissions needed as a function. Assuming that J MTs transmit during an epoch and they pick one of two power levels independently, the number of MTs choosing each power level is defined by a binomial distribution. The number of MTs transmitting using a power level (q_1) and power level 2 (q_2) can be represented using power distribution vector $\mathbf{Q} = [q_1, q_2]$. The expected number of data slots used in an epoch with a power distribution vector \mathbf{Q} can be calculated using

$$\mathbb{E}\{\Phi|\mathbf{Q}\} = \sum_{l=1}^L l \mathbb{P}\{\Phi = l|\mathbf{Q}\}, \quad (3.12)$$

where $\mathbb{P}\{\Phi = l|\mathbf{Q}\} = \prod_{m=1}^{l-1} \varepsilon(\mathbf{Q}, m)(1 - \varepsilon(\mathbf{Q}, l))$ represents the probability of having an epoch with a power distribution vector \mathbf{Q} using l data slots until having successful reception of all packets and $\varepsilon(\mathbf{Q}, m) = 1 - \prod_{i=1}^p (1 - \text{PER}_i)$. This model is extended and explained on chapter 4.

Figure 3.6 depicts the results obtained with both simulated and estimated PER values. It is clear that the results are very similar. Figure 3.7 depicts the relative and absolute error of the results presented on figure 3.6. The absolute error tends to increase with the number of MTs; on the other hand, the relative error decreases with J , making the approximate model results reasonable.

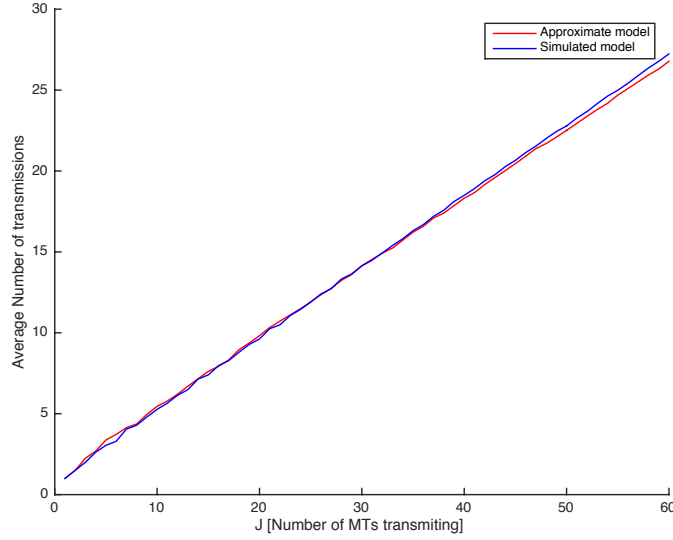


Figure 3.6: Average number of transmissions for $J = [1, 60]$

3.4 Medium access control protocol requirements

The results presented throughout this chapter can be used to extract a set of objective conditions that should be satisfied by the MAC protocol so that the system can operate in its optimal point. When only one MT is transmitting, the set up should allow the

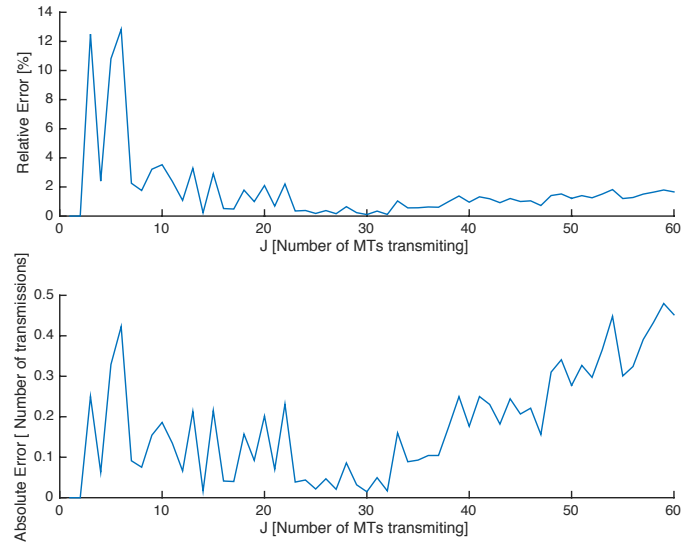


Figure 3.7: Relative error between models' average number of transmission evaluation

device to successfully send data to the BS with a single transmission. When many MTs try to send packets concurrently to the BS, the time redundancy may be used in order to successfully receive the packets.

In order to optimize the networks capacity, the MAC protocol must consider two (or more) power levels, and comprehensively allocate MTs between those levels in order to minimize the number of slots used.

As seen before, energy usage plays a big role in MTC communications, the MAC protocol must force devices to operate using minimum power.

MACHINE TYPE COMMUNICATIONS HYBRID NETWORK DIVERSITY MULTIPLE ACCESS PROTOCOL

4.1 Introduction

This chapter presents the MTC H-NDMA protocol. It starts by a small characterization of the protocol's design. After that, the simulation results are presented and validated by comparing with theoretical expectations.

4.2 Protocol design

4.2.1 Objectives

The protocol was developed to achieve three main goals:

- Allow MTC devices to operate using minimum power, making battery lives longer;
- Sub-millisecond packet transmission delay;
- High scalability.

MTC H-NDMA adapts [H-NDMA](#) protocol [24] (described in section 2.4.4) to provide [Extreme low latency \(ELL\)](#) for MTC services and advanced power savings mechanisms. The MTC H-NDMA was inspired in H-NDMA [24], uses a wake-up radio approach and cuts the number of control packets exchanged between the MTs and BS in order to allow power saving and to minimize the delay.

The following sections describe all the measures taken to comply with each objective and how [H-NDMA](#) was modified in order to design a protocol that could fulfil these goals.

4.2.2 Protocol characterization

MTC H-NDMA protocol is a random access protocol optimized to support power saving and efficient MPR interactions. It inherits the epoch concept from H-NDMA - when a new set of MTs starts transmitting, other MTs are blocked from starting transmissions until the end of the reception of the first set; the epoch is defined by the contiguous set of data slots where the MTs continue transmitting the same packets until reaching success or the maximum number of retransmissions. Unlike H-NDMA, no intermediate partial acknowledgements are sent. Instead, and like in NDMA, a tone is transmitted by the BS to signal that new retransmissions are required during an epoch. At any time, the BS may interrupt an epoch turning the tone off. At the end of an epoch, the BS generates a synchronization (SYNC) control frame, which acknowledges the packets received in the previous epoch, and defines access specific parameters for the next one.

An epoch may start asynchronously, when a MT finds the medium idle (no tone); or it may start synchronously, after the BS signals the end of an epoch by turning the tone off, just before sending the SYNC control frame. Thus, a wake-up radio method can be implemented to enhance MT's power saving. The device can use a low power secondary radio to receive the tone, and turn the main radio off while they are waiting for the SYNC frame. Figure 4.1 depicts an example of this procedure, where the main radio stays off until a SYNC packet is captured by the secondary radio

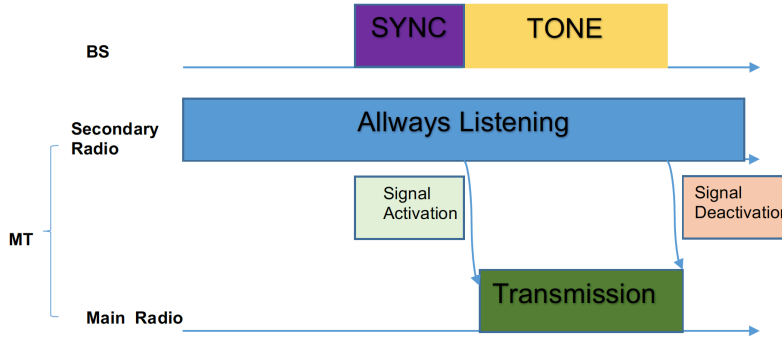


Figure 4.1: MTs wake-up radio example

The MAC protocol's algorithm operation is illustrated in figure 4.2, showing a sequence of two epochs for a system with three MTs and one BS. The first epoch starts asynchronously with a single MT transmitting, whereas the second one starts synchronized by the BS' turning off tone and runs MPR. Contrarily to NDMA, the BS runs the receiver's algorithm for each additional data slot. In this example, the BS ended the epoch after three data slots, when all packets were correctly received.

The main scalability limitation of this protocol comes from the requirement to have channels estimation. Before the transmission of the sequence of data frames in data slots, each MT transmits a physical layer header (HDR) that contains a pilot signal, which will be used to estimate the channel. In order to receive all the pilots transmitted concurrently,

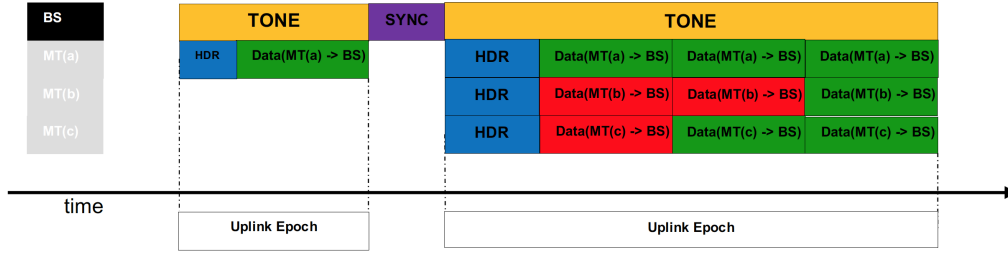


Figure 4.2: MTC H-NDMA protocol example

HDR are spread using unique orthogonal sequences, assigned to each MT by the BS during an initial association phase. Therefore, the HDR length grows linearly with the number of MTs registered in the channel. The SYNC frame also includes an acknowledgement bit mask, which also grows linearly with the number of MTs registered. On the other hand, compared to CDMA, the length of the sequence of data frames transmitted during an epoch grows much slower due to the gain achieved by using IB-DFE, power and space multiplexing.

4.2.3 Packet structure

This section describes the packets defined, their structure and the specific task they fulfill in the system.

4.2.3.1 Synchronization packet

The SYNC is a packet broadcasted by the BS to signal the end and/or beginning of an epoch. It also confirms the reception of the packets sent by the MTs during the previous epoch, and defines access specific parameters for the next one. The main SYNC's fields

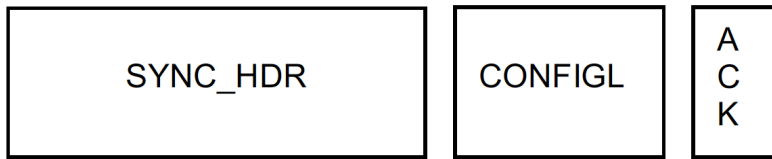


Figure 4.3: MTC H-NDMA protocol example

are:

- SYNC Header (SYNCHDR): BS' ID, pilot channel information;
- Configuration List (CONFIGL): Includes the number of transmission powers and the rules to be used;
- Acknowledgment (ACK): A bit field that acknowledges the packets received in the previous epoch.

4.2.3.2 Data packet

DATA packets contain the information the MTC devices want to transmit. Finally a Header (HDR) that contains a pilot signal, used to estimate the channel transmitted using the [Terminal Unique Orthogonal spreading-Sequence \(TUOS\)](#), is added on the first transmission within an epoch.

4.2.4 Power Control

During the association phase, the MTs receive the [TUOS](#) and a list of possible signal-to-noise ratio (SNR) required per MT, and measure the path loss to the BS. When transmitting a packet, the MTs select a random power level from the list received during the initial association, which can be managed by the BS using the SYNC frames, for instance to handle load peaks.

4.3 Performance Analysis

This section proposes an analytical model for the delay, considering guaranteed and average performance. The following modelling conditions and parameters were considered:

- a) Finite population: A finite number of J independent MTs transmit data frames containing one packet to a BS. Terminals can store an infinite number of packets.
- b) The PHY header is successfully received by the BS.
- c) The BS defines N receiver power levels, which are selected independently by the MTs when they transmit.
- d) Short delayed feedback: By the end of each slot, after a short inter-frame space (SIFS) time (i.e. T_{SIFS}), the BS has run the receiver algorithm and informs the MTs about the end of an epoch, turning off the receiver's tone and sending a SYNC frame.
- e) L defines the maximum number of data frames that each MT may transmit during an epoch.

Assuming a bit mask with K bits in the SYNC frame and a data frame duration of T_D with B bits per frame, we define the SYNC and PHY header lengths respectively as $T_{SY} = \frac{8+K}{B} T_D$ and $T_H = \frac{8K}{B} T_D$.

4.3.1 Analytical system model

4.3.1.1 Peak Performance

The service delay depends on the epoch duration, which grows with the number of MTs associated to the BS and the number of transmitting ones. Considering that P MTs transmit during an epoch and that they pick a random power level independently with probability

$1/N$, the number of MTs choosing each power level is defined by a multinomial distribution and the probability of having a power distribution vector $\mathbf{Q} = [q_1, \dots, q_N]$, with q_1 MTs at the first power level, q_2 at the second, ..., and q_N at the N th is

$$\mathbb{P}\{\mathbf{Q} = [q_1, \dots, q_N] | P\} = \frac{P!}{q_1! q_2! \dots q_N!} \left(\frac{1}{N}\right)^P. \quad (4.1)$$

The probability of having an epoch with a power distribution vector \mathbf{Q} using l data slots until having successful reception of all packets is

$$\mathbb{P}\{\Phi = l | \mathbf{Q}\} = \prod_{m=1}^{l-1} \varepsilon(\mathbf{Q}, m) (1 - \varepsilon(\mathbf{Q}, l)), \quad (4.2)$$

where $\varepsilon(\mathbf{Q}, l)$ denotes the probability of existing an error in one or more packets received from the MTs after l transmissions, calculated using $\varepsilon(\mathbf{Q}, m) = 1 - \prod_{i=1}^m (1 - \text{PER}_i)$ considering m transmissions and (3.8). It should be noticed that when multiple spatial independent paths exist, the number of retransmissions are reduced proportionally. Although the power received at each antenna is not controlled, given that it depends of the spatial distribution of the MTs in relation to each antenna (or BS, when coordinated multipoint uplink reception is used). The expected number of data slots used in an epoch with a power distribution vector \mathbf{Q} can be calculated using 4.4.

It was shown in chapter 3 that when the power received at the BS can be controlled, the power separation between the power levels is enough to make them independent and the lowest power level satisfy the minimum PER requirement, $\mathbb{E}\{\Phi | \mathbf{Q}\}$ is conditioned mainly by the maximum value of $q_n, n = 1..N$. The worst delay occurs when all MTs transmit with the same power level. In this case, the number of data slots used in an epoch is at most the highest q_n value [22], so

$$\mathbb{E}\{\Phi | \mathbf{Q} = [q_1, \dots, q_N]\} \leq \max\{q_n, n = 1..N\}. \quad (4.3)$$

The expected number of data slots until having successful reception of all packets can be calculated using

$$\mathbb{E}[\Phi | P] = \sum_{q_1=0}^P \sum_{q_2=0}^{P-q_1} \dots \sum_{q_{N-1}=0}^{P-\sum_{m=1}^{N-2} q_m} \mathbb{E}\{\Phi | \mathbf{Q}\} \mathbb{P}\{\mathbf{Q} | P\}, \quad (4.4)$$

with $\mathbf{Q} = [q_1, \dots, q_{N-1}, P - \sum_{m=1}^{N-1} q_m]$.

An epoch duration is a function of Φ following

$$\delta(\Phi) = \begin{cases} T_{SY} + T_{SIFS} + T_H + \Phi T_D + T_{SIFS}, & \Phi > 0, \\ T_{SY} + T_{SIFS} + T_{SIFS}, & \Phi = 0 \end{cases} \quad (4.5)$$

and grows with the number of MTs in a cell. The maximum service time δ_{\max} imposes a maximum number of Data slots per epoch, denoted by Φ_{\max} , which satisfy $\delta(\Phi) = \delta_{\max}$,

$$\Phi_{\max} = \left\lfloor \frac{\delta_{\max} - T_{SY} - T_H - 2T_{SIFS}}{T_D} \right\rfloor, \quad (4.6)$$

where $\lfloor \cdot \rfloor$ represents the floor operation. When hard delay guarantees are required, the number of data slots (L) can be limited to Φ_{\max} . On the other hand, this would introduce a significant restriction to the system scale. Assuming a number of slots equals to the number of MTs, i.e. $K = J$, the maximum value for J would be

$$J < \frac{(\delta_{\max} - 2T_{SIFS}) \frac{1}{T_D} - \frac{8}{B}}{\frac{9}{B} + 1}. \quad (4.7)$$

For $\delta_{\max} = 100\mu s$, considering a block with $B = 512$ bits and a duration of $4.8\mu s$, the strict upper value of J would be 20 MTs. However, the probability of occurring this power distribution condition (only one power used with N power levels defined) is very low ($1/N^{(P-1)}$).

A more tolerant approach is to let the number of slots go above Φ_{\max} with a maximum probability ϵ_M , providing support for a higher number of MTs. The probability of an epoch with P MTs transmitting exceeding the duration limit, $\epsilon_\delta(P)$, can be calculated using,

$$\epsilon_\delta(P) = \sum_{q_1=0}^P \sum_{q_2=0}^{P-q_1} \dots \sum_{q_{N-1}=0}^{P-\sum_{m=1}^{N-2} q_m} \epsilon(\mathbf{Q}, \Phi_{\max}) \mathbb{P}\{\mathbf{Q} | P\}. \quad (4.8)$$

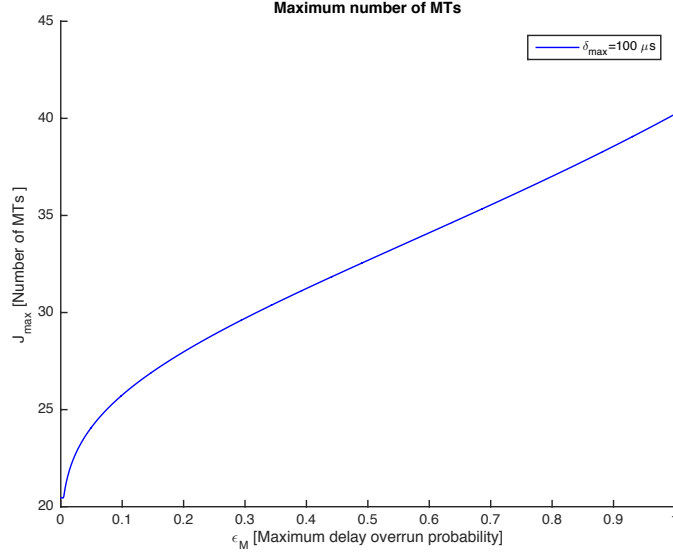
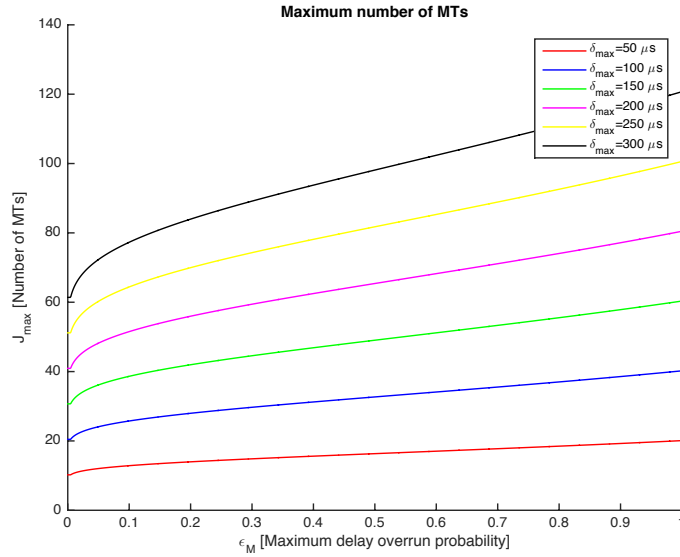
Let's consider the case when P is large and only two reception power levels are used (i.e. $N = 2$), where the binomial distribution can be approximated by the normal distribution $\mathcal{N}(P/2, P/4)$. In this case, the maximum J becomes

$$J < \frac{(\delta_{\max} - 2T_{SIFS}) \frac{1}{T_D} - \frac{8}{B}}{\frac{9}{B} + \min\left\{1; \frac{1}{2} + \frac{1}{4}\text{erf}^{-1}(1 - \epsilon_M)\right\}}, \quad (4.9)$$

where erf^{-1} denotes the inverse of the Normal's error function. In the conditions above and $\epsilon_M = 2\%$, J upper bound increases to 22 MTs as depicted in figure 4.4.

Figure 4.5 presents the evolution of maximum J with ϵ_M for different values of δ_{\max} . As expected from 4.9, J grows with the epoch duration.

The scalability of the system can be increased by using more receiving power levels. Scalability can also be increased using more antennas at the receiver, or using coordinated multipoint reception at several BSs. This creates more channels that do not require additional time slots. However, the power received from the MTs is less controlled, and some performance may be lost while using receiving power level diversity because separation is no longer guaranteed.


 Figure 4.4: Maximum J for $\delta_{\max} = 100\mu\text{s}$

 Figure 4.5: Maximum J for $\delta_{\max} \in [50, 300]\mu\text{s}$

4.3.1.2 Average performance

Poisson packet arrivals are considered to study the average performance of the system, assuming a time invariant load. Each MT receives packets that are generated with a rate λ/J packets per data slot. Therefore, the MT's queue can be modeled using a M/G/1 queue with vacations [21]. Assuming that MTs queue's are independent, the average performance of each MT can be defined based on the network's utilization rate, defined

as $\rho = \lambda \mathbb{E}[\Delta]/J$, where $\mathbb{E}[\Delta]$ is the packet's expected service time. Takács [55, pp. 66–76] showed that for a M/G/1 queue with a time-invariant service time the queue empty probability is equal to $1 - \rho$ for $\rho < 1$ and equal to 1 when the system is saturated, i.e. $\rho \geq 1$. Thus, the average service time is

$$\mathbb{E}[\Delta] = \sum_{p=0}^{J-1} \binom{J-1}{p} \rho^p (1-\rho)^{J-1-p} \delta(\mathbb{E}[\Phi | p+1]), \quad (4.10)$$

and the average epoch duration as,

$$\mathbb{E}[\zeta] = \sum_{p=1}^J \binom{J}{p} \rho^p (1-\rho)^{J-p} \delta(\mathbb{E}[\Phi | p]) + \delta(0)(1-\rho)^J. \quad (4.11)$$

An approximate value of ρ can be estimated resolving numerically the equation,

$$\rho = \frac{\lambda}{J} \mathbb{E}[\Delta](\rho). \quad (4.12)$$

Equation (4.12) has a solution in $[0, 1[$ for a non-saturated system. It assumes that all epochs end with all packets received.

4.3.1.3 Delay analysis

From the M/G/1 queue with vacation [21], the average system delay for a packet can be expressed as

$$\mathbb{E}[D] = \mathbb{E}[\Delta] + \frac{\frac{\lambda}{J} \mathbb{E}[\Delta^2]}{2(1 - \frac{\lambda}{J} \mathbb{E}[\Delta])} + \frac{\mathbb{E}[\zeta^2](J-1)}{2\mathbb{E}[\zeta](J-1)}, \quad (4.13)$$

where $\mathbb{E}[\Delta^2]$, $\mathbb{E}[\zeta](J-1)$ and $\mathbb{E}[\zeta^2](J-1)$ denote respectively the second order moment for the packet service delay, and the first moment (expected value) and the second moment of an epoch duration with $J-1$ MTs. They are defined using (4.11) and an auxiliary function for the second order moments,

$$\mathbb{E}[\delta(\Phi)^2 | P] = \sum_{q_1=0}^P \sum_{q_2=0}^{P-q_1} \dots \sum_{q_{N-1}=0}^{P-\sum_{m=1}^{N-2} q_m} \sum_{l=1}^L \delta(l)^2 \mathbb{P}\{\mathbf{Q} | P\}. \quad (4.14)$$

The second order moments are calculated using

$$\mathbb{E}[\Delta^2] = \sum_{p=0}^{J-1} \binom{J-1}{p} \rho^p (1-\rho)^{J-1-p} \mathbb{E}[\delta(\Phi)^2 | p+1], \quad (4.15)$$

$$\mathbb{E}[\zeta^2] = \sum_{p=0}^J \binom{J}{p} \rho^p (1-\rho)^{J-p} \mathbb{E}[\delta(\Phi)^2 | p]. \quad (4.16)$$

4.3.1.4 Time Limit Overrun

Besides average packet delay, ELL services introduce the necessity to estimate the probability of exceeding the latency upper bound δ_{\max} , denoted by Θ , which is equal to

$$\Theta = \sum_{p=0}^J \binom{J}{p} \rho^p (1-\rho)^{J-p} \varepsilon_{\delta}(p). \quad (4.17)$$

Θ can be kept below a probability bound ϵ_D by imposing limits to the system load, which reduce the average number of MTs transmitting per epoch.

4.3.1.5 Energy analysis

A relative measurement is proposed for the average energy used by MTs to transmit a packet during an epoch, which considers the energy per bit to noise power spectral density ratio at the receiver (obfuscating the path loss due to the distances between the MT and the BS). We start by defining the conditional average energy for an epoch with P MTs transmitting with the power levels defined by \mathbf{Q} ,

$$\begin{aligned} \mathbb{E}\{W \mid \mathbf{Q} = [q_1, \dots, q_N]\} = \\ (T_H + \mathbb{E}\{\Phi \mid \mathbf{Q}\} T_D) \frac{1}{P} \sum_{n=1}^N \frac{E_b^n}{N_0} q_n, \end{aligned} \quad (4.18)$$

where E_b^n/N_0 denotes the energy per bit to noise power spectral density ratio for power level n . The expected energy used per packet for an epoch with P MTs is

$$\begin{aligned} \mathbb{E}[W \mid P] = \\ \sum_{q_1=0}^P \sum_{q_2=0}^{P-q_1} \dots \sum_{q_{N-1}=0}^{P-\sum_{m=1}^{N-2} q_m} \mathbb{E}\{W \mid \mathbf{Q}\} \mathbb{P}\{\mathbf{Q} \mid P\}. \end{aligned} \quad (4.19)$$

Finally, the average energy used by a MT to transmit a packet during an epoch is

$$\mathbb{E}[W] = \sum_{p=0}^{J-1} \binom{J-1}{p} \rho^p (1-\rho)^{J-1-p} \mathbb{E}[W \mid p+1]. \quad (4.20)$$

4.4 Simulation Results

This section presents a set of performance results for the system considering 4 IB-DFE iterations and one antenna for the MTs and the BS. Each packet has 512 bytes and is transmitted using quadrature phase-shift keying (QPSK) in a block with a duration of 4.8 μs , including a CP with 0.8 μs . A frequency and time selective channel was considered with 16 equal power rays, spread uniformly over the CP duration.

4.4.1 Simulation scenario

System performance was measured in a micro-cell topology where the MT's distances to the BS were 5 meters ¹ and the J MTs were separated in an equiangular style, with $N = 2$ power levels, $K = J$ and $L = \lceil 0.7J \rceil$, where $\lceil \cdot \rceil$ denotes the ceil operation. MTs generate Poisson traffic with a mean λ_{MT} common for all MTs. Therefore, the aggregate load is

$$\lambda = \lambda_{\text{MT}}P. \quad (4.21)$$

Two E_b/N_0 values were selected: 16dB and 30dB. These values are slightly higher than the upper E_b/N_0 value and the $E_b/N_0 - offset$ measured in section 3.3.1 (respectively 25 dB and 13dB for a PER of 10^{-4}) to tolerate channel variations and higher interference originated by more MTs (i.e. higher J). All simulation results for $J > 60$ were compared with analytical models obtained using the approximate PER model, which was presented in chapter 3, since the computation time to evaluate the exact average PER values for all possible states proved to be very long. Without the approximate model it would not be possible to present in this dissertation simulation results for larger J .

The simulations had a duration of 10000 data slot times, where the first and last 1000 were discarded.

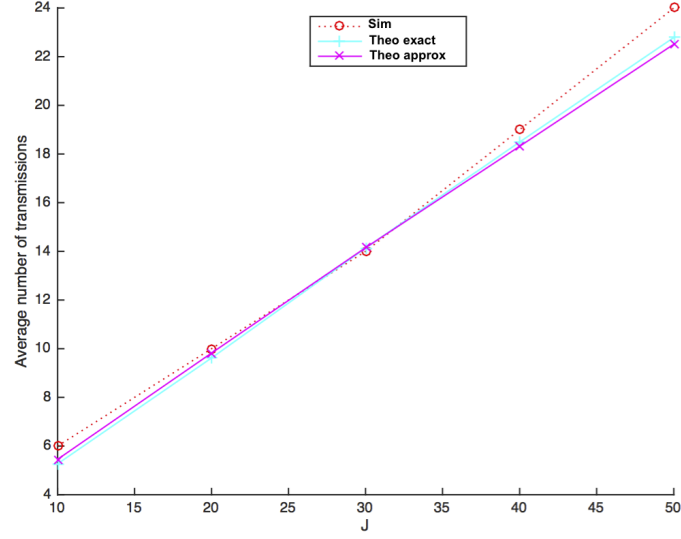
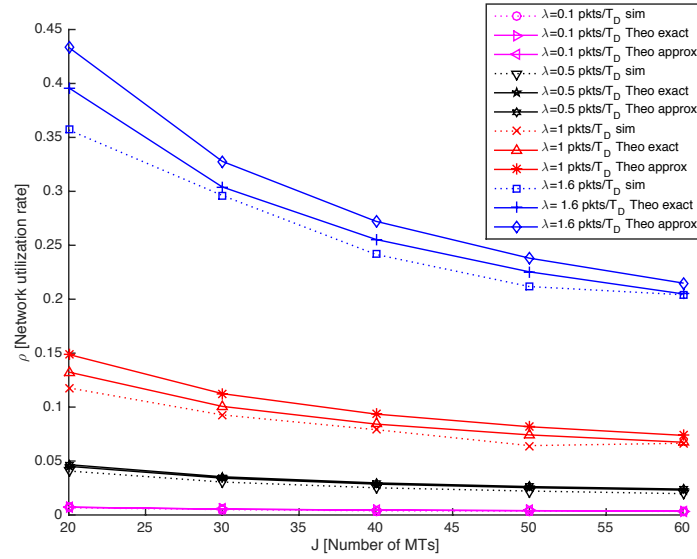
4.4.2 Average number of transmissions

Figure 4.6 shows the average number of transmissions per epoch as a function of the number of MTs $J = \{10, 20, 30, 50\}$. The model is validated and it is clear that the number of transmissions grows linearly with J .

4.4.3 Network Utilization rate

Figures 4.7 and 4.8 depict respectively the network average utilization ratio ρ and the average number of MTs that transmit during an epoch, as a function of the number of MTs for $\lambda = \{0.1, 0.5, 1, 1.6\}$ packets/ T_D . They show that the results obtained by simulation follow the ones obtained using the system model, proving its validity. As expected, the figures show that ρ and the number of MTs per epoch grow with the increase of the load. The figures show that the system is not saturated with a total load of $\lambda = 1.6$ of the capacity of a raw channel (i.e. $\rho < 1$ for $\lambda = 1.6$ packets/ T_D). Notice that the potential total capacity is almost doubled due to using two power levels; it is increased by the IB-DFE gain, but the effective capacity is reduced by the MTC H-NDMA MAC protocol overhead. The variation with the increase of the number of MTs depend on the load: for low loads (0.1 and 0.5 packets/ T_D), the two measurements almost do not change; on the other hand, for the two higher loads considered, the number of MTs transmitting per epoch grows

¹This model can be transparently applied to larger distance scenarios, since a perfect power control is being used, i.e. it only affects the transmission power proportionally. PER values do not vary, apart from the fading that may happen in the channel at each time, which also exists for greater distances


 Figure 4.6: Average number of transmissions per epoch for $J=[10,50]$

 Figure 4.7: Network utilization ratio (ρ)

and ρ tends to decrease (because the individual load decreases more rapidly than the service time increases). Figure 4.9 depicts a similar scenario as figure 4.7 but in this case for $J = [200, 1000]$. It is visible that the simulation results follow the ones obtained using the model. The system is not saturated at $\lambda = 1.5$ packets/ T_D . Figure 4.10 presents ρ as a function of λ for $J = \{600, 1000\}$. Once again, the model is validated.

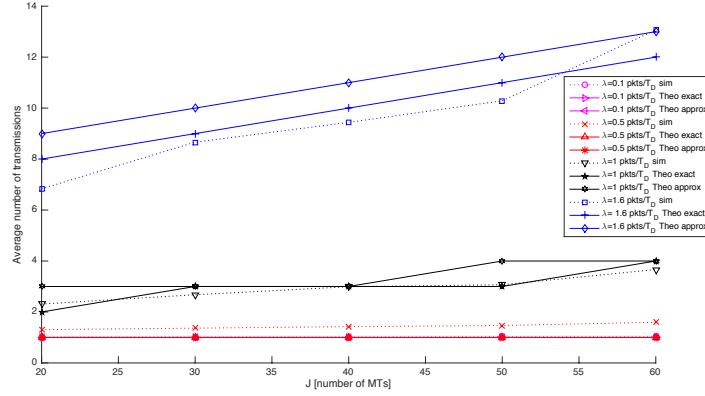


Figure 4.8: Average number of MTs per epoch

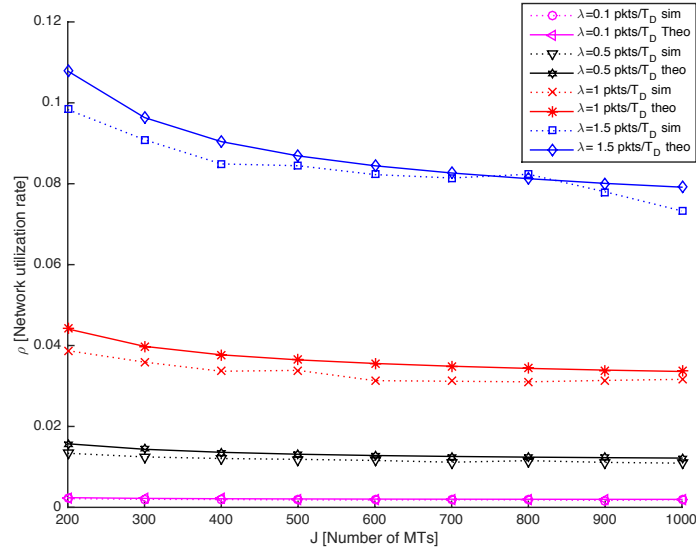
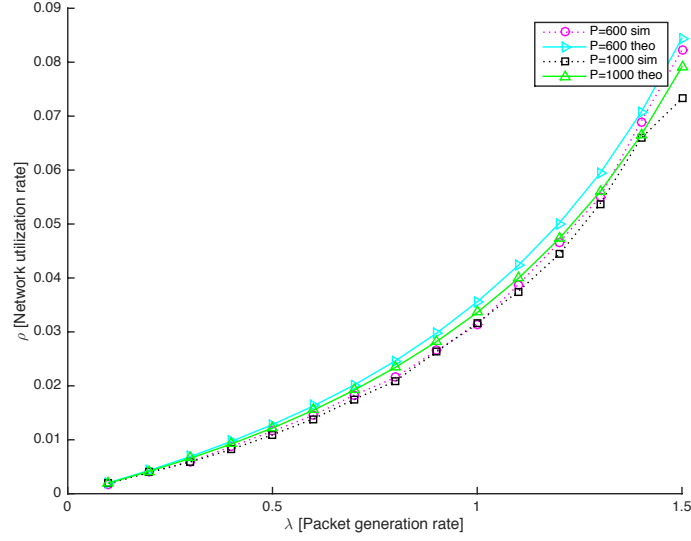
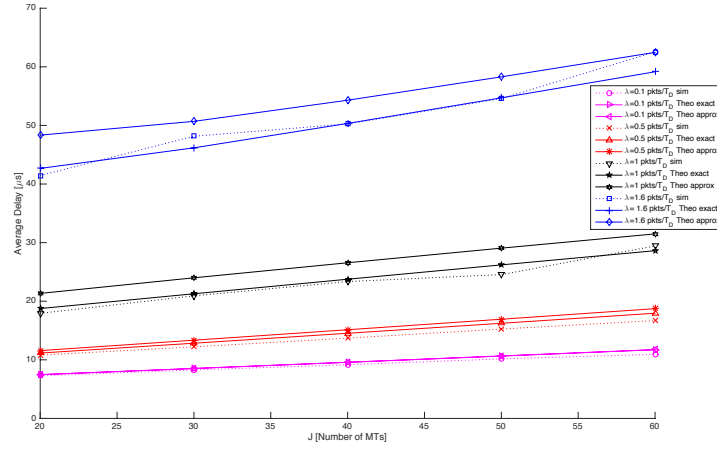


Figure 4.9: Network utilization ratio (ρ) for $J = [200, 1000]$

4.4.4 Average Delay

Figure 4.11 depicts the total average service time as a function of J , confirming again the validity of the model, although with a slight deviation for the approximated PER model, as expected. The deviation is more significant for $\lambda = 1.6$ packets/ T_D . For $\lambda = 0.1$ packets/ T_D , the variation of the total delay is due mainly to the variation of the epochs average duration. The epoch duration is equal to the packet service time, and influences the time a newly generated packet has to wait until the end of an ongoing epoch, before starting its transmission. The epoch duration increases with J because the SYNC and HDR sizes increase. For higher loads, the total delay is also influenced by the queueing delay, which is not significant for the loads considered.

Figure 4.12 presents a similar scenario, but in this case $J = [100, 1000]$ and $\lambda =$


 Figure 4.10: Network utilization ratio as a function of λ

 Figure 4.11: Average total packet delay $P=[20,60]$

$\{0.1, 1, 1.5\}$ pkts/ T_D . The same conclusions can be drawn, confirming once again the validity of the model.

Figure 4.13 presents the results in a different perspective: now the average delay appears as a function of λ . The curves depicted shows that the delay grows exponentially with the load, therefore there are some restrictions on the number of MTS that can be associated to a BS. The next section shows that it is possible to relax this restriction as long as the load is controlled.

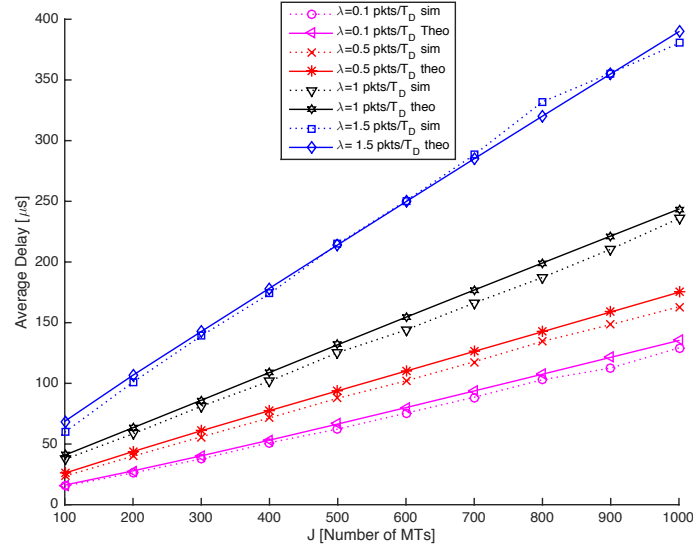


Figure 4.12: Average total packet delay $J = [100, 1000]$

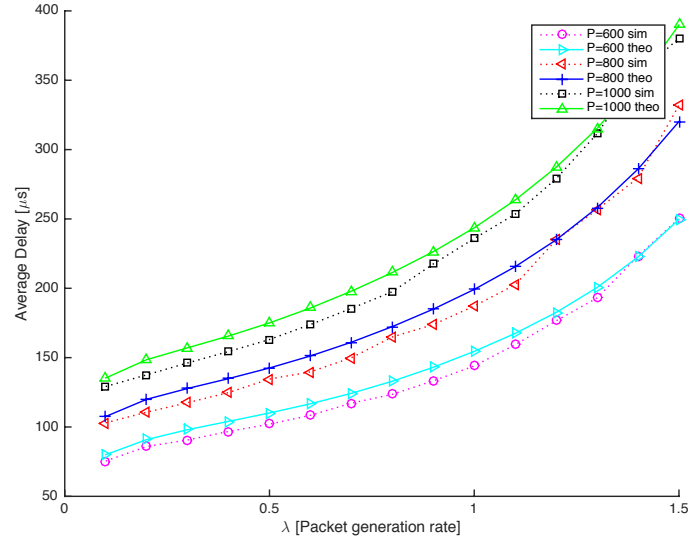


Figure 4.13: Average total packet delay as a function of λ for $J = 600, 800, 1000$

4.4.5 Time limit overrun

Figure 4.14 depicts the probability of exceeding the service time threshold value δ_{\max} . It shows that the probability is strongly influenced by the load. In section 4.3.1.1 it was shown that the service delay could be above $100 \mu\text{s}$ for $J > 20$ MTs. This figure shows that it is possible to provide ELL for more than 20 MTs, as long as the total load remains controlled. The step shape curves result from the data slot length of $T_D = 4.8 \mu\text{s}$, because Φ_{\max} is only incremented in (4.17) when the maximum time is incremented at least a

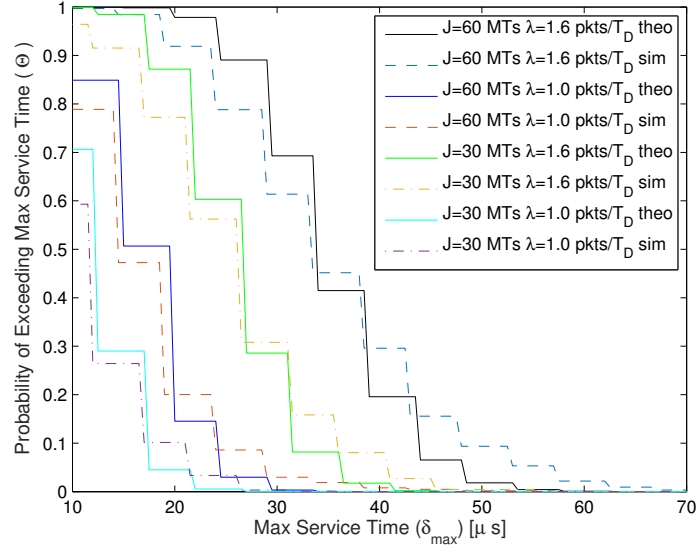


Figure 4.14: Probability of exceeding δ_{\max} for $J = \{30, 60\}$ MTs and $\lambda = \{1.0, 1.6\}$ packets/ T_D

data slot length. There is a visible deviation in the probability curves, which are more noticeable for the configurations where the average delay deviation were higher (see fig. 4.11). The theoretical model underestimates the maximum deviations measured in the simulation, mainly due to considering the average ρ value, not modelling its variation in time. Anyway, the theoretical model and the simulation results present a similar variation with δ_{\max} , and can be used to estimate it. Figure 4.15 shows the same analysis but for

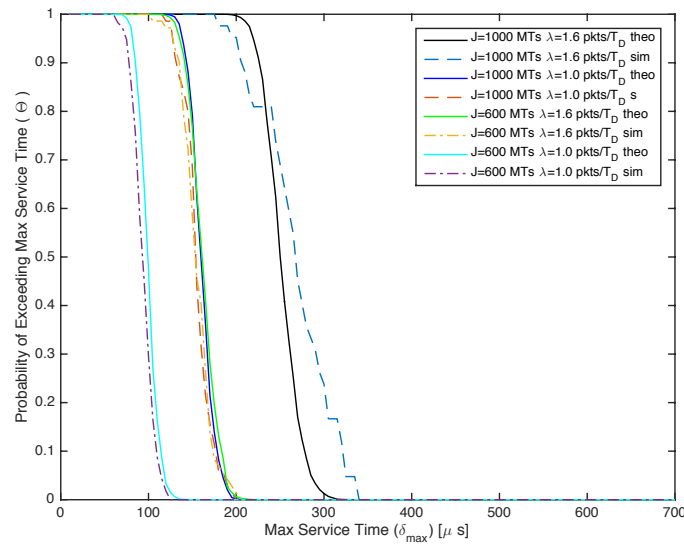


Figure 4.15: Probability of exceeding δ_{\max} for $J = \{600, 1000\}$ MTs and $\lambda = \{1.0, 1.6\}$ packets/ T_D

higher values of J . It provides the same conclusions and shows that the system is able to provide ELL for higher values of J .

4.4.6 Energy efficiency

This section presents the system performance in terms of energy efficiency. Figure 4.16 presents the **Energy Per Useful Packet (EPUP)** as a function of J , calculated using 4.20. There is some deviation between the results due to variations on the simulated number of transmissions per epoch, but the validity of the model is confirmed. It is clear that the curves are logarithmic, therefore if the load is controlled, the energy used for packet transmission grows slowly with J , a very positive result in a MTC environment.

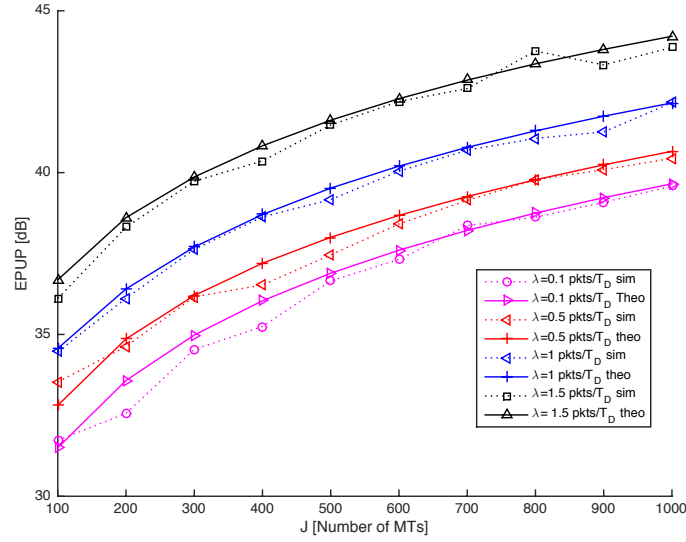


Figure 4.16: EPUP as a function of J

CONCLUSIONS

5.1 Final considerations

This dissertation focused on proposing an adaptation of the H-NDMA protocol to provide ELL for MTC services and advanced power saving mechanisms. Chapter 2 characterized the most significant access schemes and existing M2M MAC protocols, and presented a group of MPR techniques showing the potential they have for MTC communications. Chapter 3 analyzed the MPR receiver, showing the advantages of implementing multiple power levels for MTs data transmission. The results showed that for all combinations of number of MTs distributed between power levels there are E_b/N_0 and number of data slots above which the system is capable of successfully receive the packets, showing also that with the offset of -12 dB between power levels, the receiver using two power levels requires much less data slots for the same number of MTs. Finally, it validates an simplified model for large systems. Chapter 4 characterized the protocol and analysed the system level performance, which was validated using a system level simulator that runs the physical layer receiver model. Although the strict ELL guarantees restrict significantly the number of MTs that can be associated to a BS, this dissertation shows that it is possible to relax this restriction and still provide ELL as long as the total load is controlled in the MTC network. Finally, this dissertation also shows that the EPUP as a function of J is a logarithmic curve. Therefore if the load is controlled, the energy used for packet transmission grows slowly with J , a very positive result in a MTC environment.

5.2 Future work

Future work, that will not be added to this dissertation, includes the study of the performance of GFDM MPR receiver, the adaptation of the MTC H-NDMA MAC protocol in

order to cope with this new scenario and the implementation of a cross-layer PHY and network layer simulator for the GFDM system.

BIBLIOGRAPHY

- [1] T. R. 3GPP. “3GPP TR 36.814, 3rd Generation Partnership Project; Technical Specification Group RAN1; Further Advancements for E-UTRA Physical Layer Aspects”. In: 2010.
- [2] M. Al-imari, P. Xiao, M. A. Imran, and R. Tafazolli. “Uplink Non-Orthogonal Multiple Access for 5G Wireless Networks”. In: *Wireless Communications Systems (ISWCS), 2014 11th International Symposium* (2014), pp. 781–785.
- [3] A.Lo, Y.W.Law, M.Jacobson, and M.Kucharzak. “Enhanced LTE-Advanced random-access mechanism for massive machine-to-machine (M2M) communications”. In: *Proc.WWRF* (2011), pp. 1–5.
- [4] J. Andrews. “Modulation, coding and signal processing for wireless communications - Interference cancellation for cellular systems: a contemporary overview”. In: *IEEE Wireless Communications* 12.2 (2005), pp. 19–29.
- [5] F. V Azquez-Gallego, J. Alonso-Zarate, I. Balboteo, and L. Alonso. “DPCF-M: A Medium Access Control protocol for dense Machine-to-Machine area networks with dynamic gateways”. English. In: *2013 IEEE 14th Workshop on Signal Processing Advances in Wireless Communications (SPAWC)*. IEEE, 2013, pp. 490–494.
- [6] J.-J. van de Beek, O. Edfors, M. Sandell, S. Wilson, and P. Borjesson. “On channel estimation in OFDM systems”. English. In: *1995 IEEE 45th Vehicular Technology Conference. Countdown to the Wireless Twenty-First Century*. Vol. 2. IEEE, pp. 815–819.
- [7] N. Benvenuto and S. Tomasin. “Block iterative DFE for single carrier modulation”. In: *Electronics Letters* 38.19 (2002), p. 1144.
- [8] N. Benvenuto and S. Tomasin. “On the comparison between OFDM and single carrier modulation with a DFE using a frequency-domain feedforward filter”. In: *IEEE Transactions on Communications* 50.6 (2002), pp. 947–955.
- [9] N. Benvenuto and S. Tomasin. “Iterative Design and Detection of a DFE in the Frequency Domain”. In: *IEEE Transactions on Communications* 53.11 (2005), pp. 1867–1875.

- [10] N Benvenuto, R Dinis, D Falconer, and S Tomasin. "Single Carrier Modulation With Nonlinear Frequency Domain Equalization: An Idea Whose Time Has Come - Again". In: *Proceedings of the IEEE* 98.1 (2010), pp. 69–96.
- [11] M. Bossert, A. Donder, and V. Zyablov. "Improved channel estimation with decision feedback for OFDM systems". In: *Electronics Letters* 34.11 (1998), p. 1064.
- [12] Y. Chen and W. Wang. "Machine-to-Machine Communication in LTE-A". In: *2010 IEEE 72nd Vehicular Technology Conference - Fall*. IEEE, 2010, pp. 1–4.
- [13] M. Debbah. "Short introduction to OFDM". In: *White Paper, Mobile Communications Group, Institut Eurocom* (2004).
- [14] L. Deneire, B. Gyselinckx, and M. Engels. "Training sequence versus cyclic prefix-a new look on single carrier communication". In: *IEEE Communications Letters* 5.7 (2001), pp. 292–294.
- [15] D. Falconer, S. Ariyavisitakul, A. Benyamin-Seeyar, and B. Eidson. "Frequency domain equalization for single-carrier broadband wireless systems". In: *IEEE Communications Magazine* 40.4 (2002), pp. 58–66.
- [16] B. Farhang-Boroujeny and R. Kempter. "Multicarrier communication techniques for spectrum sensing and communication in cognitive radios". In: *IEEE Communications Magazine* 46.4 (2008), pp. 80–85.
- [17] B. Farhang-Boroujeny. "OFDM Versus Filter Bank Multicarrier". In: *IEEE Signal Processing Magazine* 28.3 (2011), pp. 92–112.
- [18] G. Fettweis and S. Alamouti. "5G: Personal mobile internet beyond what cellular did to telephony". In: *IEEE Communications Magazine* 52.2 (2014), pp. 140–145.
- [19] G. P. Fettweis. "The Tactile Internet: Applications and Challenges". In: *IEEE Vehicular Technology Magazine* 9.1 (2014), pp. 64–70.
- [20] G. Fettweis. "A 5G wireless communications vision". In: *Microwave Journal* (2012).
- [21] R. Gallager and D. Bertsekas. *Data Networks 2nd Edition*. Prentice Hall, 2004.
- [22] F Ganhao and R Dinis. "Analytical BER and PER performance of frequency-domain diversity combining, multipacket detection and hybrid schemes". In: ... , *IEEE Transactions on* 60.8 (2012), pp. 2353–2362.
- [23] F. Ganhao, M. Pereira, L. Bernardo, R. Dinis, R. Oliveira, and P. Pinto. "Performance of Hybrid ARQ for Network Diversity Multiple Access Schemes". English. In: *2011 Proceedings of 20th International Conference on Computer Communications and Networks (ICCCN)*. IEEE, 2011, pp. 1–6.
- [24] F. Ganhão, M. Pereira, L. Bernardo, R. Dinis, R. Oliveira, and P. Pinto. "Performance Analysis of an Hybrid ARQ Adaptation of NDMA Schemes". In: *IEEE Transactions on Communications* 61.8 (2013), pp. 3304–3317.

-
- [25] F. Ganhao, L. Bernardo, R. Dinis, R. Oliveira, and P. Pinto. "Uplink Performance Evaluation of Packet Combining ARQ for MPR Prefix-Assisted DS-CDMA". In: *IEEE Transactions on Communications* 63.7 (2015), pp. 2685–2697.
 - [26] I. Gaspar, N. Michailow, A. Navarro, E. Ohlmer, S. Krone, and G. Fettweis. "Low Complexity GFDM Receiver Based on Sparse Frequency Domain Processing". In: *2013 IEEE 77th Vehicular Technology Conference (VTC Spring)* (2013), pp. 1–6.
 - [27] Guo Wang, Xiaofeng Zhong, Shunliang Mei, and Jing Wang. "An adaptive medium access control mechanism for cellular based Machine to Machine (M2M) communication". In: *2010 IEEE International Conference on Wireless Information Technology and Systems*. IEEE, 2010, pp. 1–4.
 - [28] S. Henrik and L. Christian. *OFDM and CDMA : Theory and Applications - Wideband Wireless Communications*. 2005.
 - [29] C.-Y. Hsu, C.-H. Yen, and C.-T. Chou. "An adaptive multichannel protocol for large-scale machine-to-machine (M2M) networks". In: *2013 9th International Wireless Communications and Mobile Computing Conference (IWCMC)*. IEEE, 2013, pp. 1223–1228.
 - [30] IEEE. "Wireless LAN Medium Access Control (MAC) and Physical Layer (PHY) Specifications". In: *ANSI/IEEE Std 802.11, 1999 Edition (R2003)* (2003), pp. i–513.
 - [31] IST-4-027756 WINNER II.D4.6.1. *The WINNER II Air Interface: Refined Multiple Access Concepts - Google Search*. 2006.
 - [32] V. Kotzsch and G. Fettweis. "Interference Analysis in Time and Frequency Asynchronous Network MIMO OFDM Systems". English. In: *2010 IEEE Wireless Communication and Networking Conference*. IEEE, 2010, pp. 1–6.
 - [33] K. Letaief. "Cross-Layer Multi-Packet Reception Based Medium Access Control and Resource Allocation for Space-Time Coded MIMO/OFDM". English. In: *IEEE Transactions on Wireless Communications* 7.9 (2008), pp. 3372–3384.
 - [34] Y. Liu. "A scalable Hybrid MAC protocol for massive M2M networks". In: *2013 IEEE Wireless Communications and Networking Conference (WCNC)*. IEEE, 2013, pp. 250–255.
 - [35] J. Lu, W. Shu, and M. Wu. "A survey on multipacket reception for wireless random access networks". In: *Journal of Computer Networks and Communications* 2012 (2012), p. 14.
 - [36] P. Marsch and G. P. Fettweis. "Coordinated Multi-Point in Mobile Communications From Theory to Practice". In: *Cambridge University Press* (2011).
 - [37] N. Mehta and A. Molisch. "Asynchronous interference mitigation in cooperative base station systems". In: *IEEE Transactions on Wireless Communications* 7.1 (2008), pp. 155–165.

- [38] N. Michailow, R. Datta, S. Krone, M. Lentmaier, and G. Fettweis. “Generalized Frequency Division Multiplexing : A Flexible Multi-Carrier Modulation Scheme for 5th Generation Cellular Networks”. In: *Proceedings of the German Microwave Conference(GeMiC’12)* 62.9 (2012), pp. 1–4.
- [39] H. Myung, J. Lim, and D. Goodman. “Single carrier FDMA for uplink wireless transmission”. English. In: *IEEE Vehicular Technology Magazine* 1.3 (2006), pp. 30–38.
- [40] R. van Nee and R. Prasad. “OFDM for Wireless Multimedia Communications”. In: 246-247 (2000).
- [41] R. Negi and J. Cioffi. “Pilot tone selection for channel estimation in a mobile OFDM system”. English. In: *IEEE Transactions on Consumer Electronics* 44.3 (1998), pp. 1122–1128.
- [42] C. W. Park, D. Hwang, and T.-J. Lee. “Enhancement of IEEE 802.11ah MAC for M2M Communications”. In: *IEEE Communications Letters* 18.7 (2014), pp. 1151–1154.
- [43] R. Pickholtz, D. Schilling, and L. Milstein. “Theory of Spread-Spectrum Communications–A Tutorial”. English. In: *IEEE Transactions on Communications* 30.5 (1982), pp. 855–884.
- [44] L Ping, L Liu, and W. Leung. “A simple approach to near-optimal multiuser detection: interleave-division multiple-access”. In: *Wireless Communications and ...* (2003).
- [45] N. K. Pratas, H. Thomsen, C. Stefanovic, and P. Popovski. “Code-expanded random access for machine-type communications”. In: *2012 IEEE Globecom Workshops*. IEEE, 2012, pp. 1681–1686.
- [46] A. Rajandekar and B. Sikdar. “A Survey of MAC Layer Issues and Protocols for Machine-to-Machine Communications”. In: *IEEE Internet of Things Journal* 2.2 (2015), pp. 175–186.
- [47] R. Rom and M. Sidi. *Multiple Access Protocols: Performance and Analysis*. 2011.
- [48] Y. Saito, Y. Kishiyama, A. Benjebbour, T. Nakamura, A. Li, and K. Higuchi. “Non-orthogonal multiple access (NOMA) for cellular future radio access”. In: *IEEE Vehicular Technology Conference* (2013), pp. 0–4.
- [49] A. Scaglione, G. Giannakis, and S. Barbarossa. “Redundant filterbank precoders and equalizers. I. Unification and optimal designs”. In: *IEEE Transactions on Signal Processing* 47.7 (1999), pp. 1988–2006.
- [50] A. Scaglione, G. Giannakis, and S. Barbarossa. “Redundant filterbank precoders and equalizers. II. Blind channel estimation, synchronization, and direct equalization”. In: *IEEE Transactions on Signal Processing* 47.7 (1999), pp. 2007–2022.

-
- [51] K. Shamaei and M. Sabbaghian. “Analytical Performance Evaluation of SC-FDMA Systems in the Presence of Frequency and Time Offset”. In: *Wireless Communications, IEEE Transactions on* 14.11 (2015), pp. 6230–6239.
 - [52] W. Stallings. *Data and Computer Communications, International Edition*. Pearson Education Limited, 2015, p. 912.
 - [53] A. Stamoulis, G. Giannakis, and A. Scaglione. “Block FIR decision-feedback equalizers for filterbank precoded transmissions with blind channel estimation capabilities”. In: *IEEE Transactions on Communications* 49.1 (2001), pp. 69–83.
 - [54] N. Tadayon and S. Aissa. “Modeling and Analysis of Cognitive Radio Based IEEE 802.22 Wireless Regional Area Networks”. In: *IEEE Transactions on Wireless Communications* 12.9 (2013), pp. 4363–4375.
 - [55] L. Takács. *Introduction to the theory of queues*. Oxford University Press, 1962, p. 268.
 - [56] M. Tsatsanis and S. Banerjee. “Network-assisted diversity for random access wireless networks”. In: *IEEE Transactions on Signal Processing* 48.3 (2000), pp. 702–711.
 - [57] D. Tse and S. Hanly. “Linear multiuser receivers: effective interference, effective bandwidth and user capacity”. In: *IEEE Trans. Inf. Theory* 45.2 (1999), pp. 641–657.
 - [58] U. Tureli and H. Liu. “Blind carrier synchronization and channel identification for OFDM communications”. English. In: *Proceedings of the 1998 IEEE International Conference on Acoustics, Speech and Signal Processing, ICASSP '98 (Cat. No.98CH36181)*. Vol. 6. IEEE, pp. 3509–3512.
 - [59] V. Vakilian, T. Wild, F. Schaich, S. ten Brink, and J.-F. Frigon. “Universal-filtered multi-carrier technique for wireless systems beyond LTE”. In: *2013 IEEE Globecom Workshops (GC Wkshps)*. IEEE, 2013, pp. 223–228.
 - [60] M. K. Varanasi and T. Guess. “Optimum decision feedback multiuser equalization with successive decoding achieves the total capacity of the Gaussian multiple-access channel”. In: *Signals, Systems and Computers, 1997. Conference Record of the Thirty-First Asilomar Conference on*. Vol. 2. 1997, 1405–1409 vol.2.
 - [61] A. J. Viterbi. *CDMA: Principles of Spread Spectrum Communication*. Addison-Wesley Publishing Company, 1995, p. 245.
 - [62] H. Wu, C. Zhu, R. J. La, X. Liu, and Y. Zhang. “Fast Adaptive S-ALOHA Scheme for Event-Driven Machine-to-Machine Communications”. In: *2012 IEEE Vehicular Technology Conference (VTC Fall)*. IEEE, 2012, pp. 1–5.

- [63] G. Wunder, P. Jung, M. Kasparick, T. Wild, F. Schaich, Y. Chen, S. T. Brink, I. Gaspar, N. Michailow, A. Festag, L. Mendes, N. Cassiau, D. Kténas, M. Dryjanski, S. Pietrzyk, B. Eged, P. Vago, and F. Wiedmann. “5G NOW: Non-orthogonal, asynchronous waveforms for future mobile applications”. In: *IEEE Communications Magazine* 52.2 (2014), pp. 97–105.



SIMULATOR'S STRUCTURE

A.1 Global architecture

The simulator's process is depicted in figure A.1. At start, the system's parameters are loaded into the simulator, creating a MATLAB object called *systemObject*. This object contains all the information about the system, defined with the following attributes:

1. *time*: the time instant the simulator is at;
2. *SYNCTime*, *DATAtime*: the duration of each control and data packet;
3. *maxTime*: maximum simulation time (used as a stop condition for the simulator);
4. *normalizedPower*: the normalized power in dB. The power levels used by the terminals are calculated in relation to this value, using the model presented in section 3;
5. *powerLevels*: Vector containing the transmission power values in dB;
6. *Niter*: number of iterations used by the IB-DFE receiver;
7. *fc*: centre frequency (in GHz);
8. *distanceMatrix*, *xiMatrix*: distance and channel coefficient matrices. The first contains the distance between MTs and to the BS, and is calculated using MTs' location information; the second one is described in section A.2;
9. *terminal*: an array of objects which contain the properties of all the terminals. The BS is always the last terminal in this array.

Each terminal is modelled by a set of technical and statistical attributes. The technical attributes characterize and define the terminal's behaviour in the system. The statistical

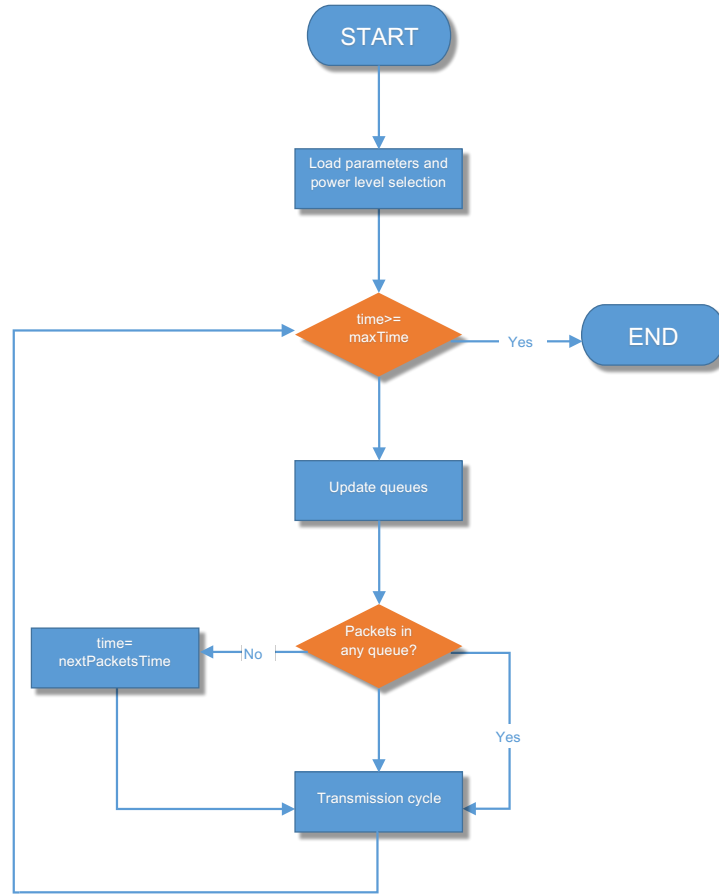


Figure A.1: Simulation flowchart

attributes allow the quantification of the terminal's performance in the system, which are used for the determination of statistical measures *a posteriori*. The technical attributes are:

- *coordinates*: geographical position of the terminal in relation to the BS;
- *directionalGain*: the gain of the antenna the terminal is using;
- *timeGenerationPackets*: array that contains the instants in which the packets are generated;
- *destination*: array that contains the destination for each packet generated. All MTs' destinations are set to the BS;
- *packetsInQueue*: number of packets still in queue;

- *idle*: Boolean variable to indicate if the terminal wants to transmit. True if *packetsInQueue* > 0.

The statistical attributes are:

- *successfulTransmissions*: number of successful transmissions. Coincides with the number of packets delivered to the terminal's destination;
- *unsuccessfulTransmission*: number of unsuccessful transmissions;
- *packetsDropped*: number of packets dropped;
- *timePacketEnteredQueue*: array that contains the instants in which the packets are added to the queue;
- *timeTransmissionStart*: array that contains the instants in which the packets start to be transmitted;
- *timeTransmissionEnd*: array that contains the instants in which the terminal ceased transmission for each packet;
- *TXpower*: array that contains the power levels used for each transmission.

After all these attributes are set, the simulator enters into a loop. At the start of each cycle, the stop condition $time > maxTime$ is checked. If false, the simulator uses the current *time* to update the queues of all terminals and checks if there are any terminals with packets pending. If there aren't, the simulator jumps to the next event ($time = nextPacketsTime$). Otherwise, the last routine, transmission cycle is run. It simulates the transmissions from MTs to the BS and updates the *time* variable.

The receptions are simulated by running several iterations of the IB-DFE receiver presented in chapter 3 for each time slot. To decide which packets get delivered, each reception's PER is compared to a uniform random number in the interval $[0, 1]$. If the PER is inferior to this number, the packet is assumed to have been delivered to its destination. With each transmission, the attributes in the *terminal* object are updated. Lastly, the *time* variable is updated by adding the duration of the control and data packets used in the transmission cycle.

A.2 Distance and channel coefficient

After all parameters are loaded, the simulator starts by calculating the distance from all terminals to the BS. This information is stored in the distance matrix. As explained in this dissertation, this protocol allows the use of many power levels, then, each terminal is given a random *offset* value from the *powerLevels* array. The channel coefficient is denoted by x_i and represent the difference to the normalized power (16dBm was considered in

this dissertation). The power that reaches the receiver in a transmission can be calculated using

$$xi = linear2db(\sqrt{db2linear(of fset(i) + G_0 + P_L(d))}), \quad (A.1)$$

where $linear2db(x)$ denotes the conversion from linear to dB, $db2linear(x)$ denotes the conversion from dB to linear, $offset(i)$ denotes difference between the power level used by terminal i , in order to reach the BS, and the normalized power level of the simulator, G_0 denotes the antenna gain and $P_L(d)$ denotes the path loss given a distance d , which is calculated using

$$P_L = -(16.9 \log_{10} d + 32.8 + 20 \log_{10} f c). \quad (A.2)$$

A.3 Output

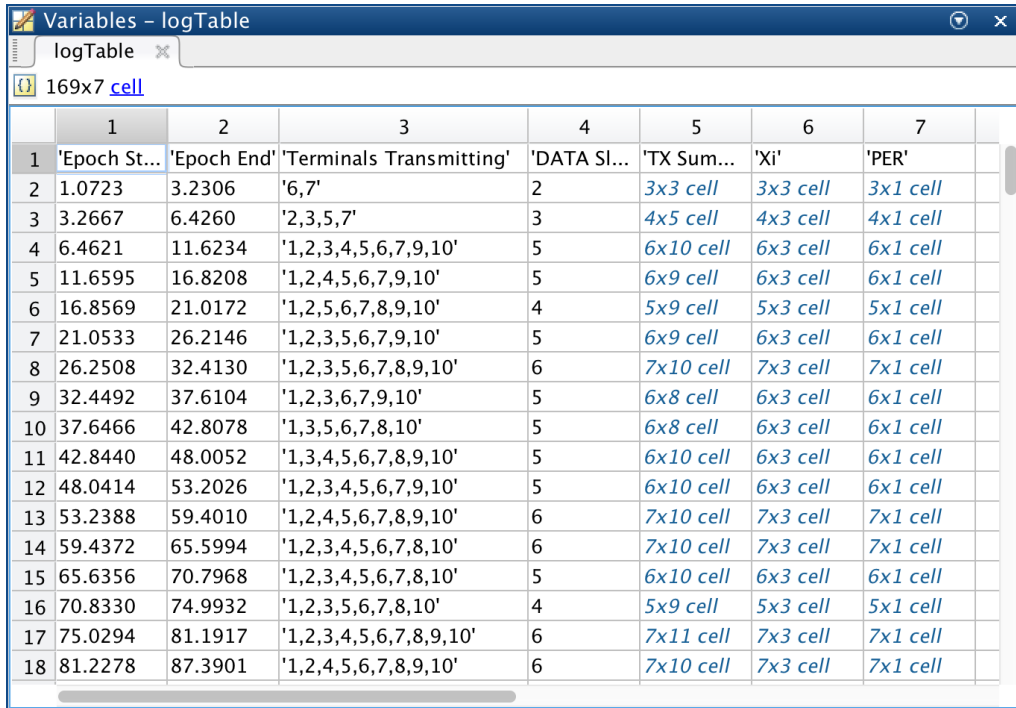
At the end of each simulation, the simulator produces two MATLAB cell arrays: *statsTable* and *logTable*. *statsTable* contains a statistical analysis of the simulation and *logTable* contains the characterization of what happened in each time slot, organized in a set of operating mode's epochs. An example of *statsTable* and *logTable* is shown in figures A.2 and A.3 respectively. The tables depicted are illustrations of the simulations used for the system analysis with 200% aggregate uplink load with 10 MTs.

Figure A.2 depicts the *statsTable* cell. The queueing delay is defined by the time a packet waits in queue and can be calculated by subtracting the time a packet starts to be transmitted to the time the packet enters the queue. The service time is defined by the time it takes for a packet to be delivered and can be calculated by subtracting the time the terminal ceases transmission for a given packet to the time a packet starts to be transmitted.

	1	2	3	4	5	6	7	8	9	10	11
1		'User 1 '	'User 2 '	'User 3 '	'User 4 '	'User 5 '	'User 6 '	'User 7 '	'User 8 '	'User 9 '	'User 10 '
2	'Min Nro. TX'	5	5	5	5	5	5	5	5	5	5
3	'Max Nro. TX'	6	7	6	6	6	5	5	7	5	7
4	'Average Nro. TX'	5.0076	5.8030	5.0076	5.0076	5.0076	5	5	5.8321	5	5.8106
5	'Min Queuing Delay'	39.1974	20.1068	14.6110	23.8316	22.4633	9.3789	5.3342	7.2903	18.5581	24.9661
6	'Max Queuing Delay'	219.2670	124.4281	225.3401	143.2374	193.3619	136.8553	76.2721	156.4202	207.4750	128.7284
7	'Average Queuing Delay'	120.4690	65.3634	130.2634	85.5055	129.1581	80.7702	24.9128	63.6065	107.9920	58.7991
8	'Min Service Time'	5.1612	5.1612	5.1612	5.1612	5.1612	5.1612	5.1612	5.1612	5.1612	5.1612
9	'Max Service Time'	6.1622	7.1632	6.1622	6.1622	6.1622	5.1613	5.1613	7.1632	5.1613	7.1632
10	'Average Service Time'	5.1688	5.9651	5.1688	5.1688	5.1688	5.1612	5.1612	5.9941	5.1612	5.9727
11	'Successful Transmissions'	132	132	132	132	132	131	127	131	132	132
12	'Unsuccessful Transmissions'	529	634	529	529	529	524	508	633	528	635
13	'Total Transmissions'	661	766	661	661	661	655	635	764	660	767
14	'Packet Delivery Ratio'	0.1997	0.1723	0.1997	0.1997	0.1997	0.2000	0.2000	0.1715	0.2000	0.1721
15	'Throughput'	0.1650	0.1650	0.1650	0.1650	0.1650	0.1638	0.1588	0.1638	0.1650	0.1650
16	'Total Energy'	43.2020	36.8423	43.2020	43.2020	43.2020	43.1624	43.0277	36.8309	43.1954	36.8480
17	'EPUP'	21.9963	15.6365	21.9963	21.9963	21.9963	21.9897	21.9897	15.6582	21.9897	15.6422

Figure A.2: *statsTable* for 10 MTs with 200% aggregate uplink load

Figure A.3 depicts the *logTable* cell. Each line represents an epoch (time interval between the two SYNCs). Its columns are:



	1	2	3	4	5	6	7
1	'Epoch St...	'Epoch End'	'Terminals Transmitting'	'DATA Sl...	'TX Sum...	'Xi'	'PER'
2	1.0723	3.2306	'6,7'	2	3x3 cell	3x3 cell	3x1 cell
3	3.2667	6.4260	'2,3,5,7'	3	4x5 cell	4x3 cell	4x1 cell
4	6.4621	11.6234	'1,2,3,4,5,6,7,9,10'	5	6x10 cell	6x3 cell	6x1 cell
5	11.6595	16.8208	'1,2,4,5,6,7,9,10'	5	6x9 cell	6x3 cell	6x1 cell
6	16.8569	21.0172	'1,2,5,6,7,8,9,10'	4	5x9 cell	5x3 cell	5x1 cell
7	21.0533	26.2146	'1,2,3,5,6,7,9,10'	5	6x9 cell	6x3 cell	6x1 cell
8	26.2508	32.4130	'1,2,3,5,6,7,8,9,10'	6	7x10 cell	7x3 cell	7x1 cell
9	32.4492	37.6104	'1,2,3,6,7,9,10'	5	6x8 cell	6x3 cell	6x1 cell
10	37.6466	42.8078	'1,3,5,6,7,8,10'	5	6x8 cell	6x3 cell	6x1 cell
11	42.8440	48.0052	'1,3,4,5,6,7,8,9,10'	5	6x10 cell	6x3 cell	6x1 cell
12	48.0414	53.2026	'1,2,3,4,5,6,7,9,10'	5	6x10 cell	6x3 cell	6x1 cell
13	53.2388	59.4010	'1,2,4,5,6,7,8,9,10'	6	7x10 cell	7x3 cell	7x1 cell
14	59.4372	65.5994	'1,2,3,4,5,6,7,8,10'	6	7x10 cell	7x3 cell	7x1 cell
15	65.6356	70.7968	'1,2,3,4,5,6,7,8,10'	5	6x10 cell	6x3 cell	6x1 cell
16	70.8330	74.9932	'1,2,3,5,6,7,8,10'	4	5x9 cell	5x3 cell	5x1 cell
17	75.0294	81.1917	'1,2,3,4,5,6,7,8,9,10'	6	7x11 cell	7x3 cell	7x1 cell
18	81.2278	87.3901	'1,2,4,5,6,7,8,9,10'	6	7x10 cell	7x3 cell	7x1 cell

Figure A.3: statsTable for 10 MTs with 200% aggregate uplink load

- Epoch Start: time the SYNC broadcast finishes;
- Epoch End: time the SYNC broadcast begins;
- Terminals Transmitting: terminals transmitting in the epoch;
- DATA Slots Used: number of slots contained in the epoch;
- TX Summary: cell that contains the successful transmissions;
- Xi: cell that contains the x_i values, used for each transmission by the MTs.
- PER: cell that contains the PER associated to each transmission.



ARTICLE

This appendix contains the reference the article accepted for publication in the *IEEE GLOBECOM 2016 Workshops*:

B Ramos, L Bernardo, R Dinis, R Oliveira, P Pinto, and P Amaral. "Using Lightly Synchronized Multipacket Reception in Machine-Type Communication Networks."In: the 3rd Int. Workshop on Ultra-Reliable Low-Latency Communications in Wireless Networks of the 2016 IEEE Global Communications Conference (Globecom'16), Washington, USA, 4-8 December 2016.